HGF induces epithelial-to-mesenchymal transition by modulating the mammalian Hippo/MST2 and ISG15 pathways

Jennifer Farrell[1], *Ciara Kelly*[2,3], *Jens Rauch*[1], *Katarzyna Kida*[1], *Amaya García-Muñoz*[1], *Naser Monsefi*[1], *Benedetta Turriziani*[1], *Carolanne Doherty*[1], *Jai P. Mehta*[1], *David Matallanas*[1], *Jeremy C. Simpson*[2,3], *Walter Kolch*[1,3,4], *Alex von Kriegsheim*[1*]

[1] Systems Biology Ireland, University College Dublin, Belfield, Dublin 4, Ireland

[2] School of Biology and Environmental Science, University College Dublin, Dublin, Ireland

[3] Conway Institute of Biomolecular & Biomedical Research, University College Dublin, Belfield, Dublin 4, Ireland

[4] School of Medicine and Medical Science, University College Dublin, Belfield, Dublin 4, Ireland

[*] To whom correspondence should be addressed

Alex von Kriegsheim
Systems Biology Ireland

University College Dublin

Belfield Campus

Dublin 4

Ireland

Tel.:+353 1 716 6326,

Fax: +353 1 716 6701

Email: alex.vonkriegsheim@ucd.ie

KEYWORDS

Epithelial mesenchymal transition, Hippo-pathway, ISG5, SILAC, quantitative expression proteomics

ABSTRACT

Epithelial to Mesenchymal Transition (EMT) is a fundamental cell differentiation/de-differentiation process which is associated with dramatic morphological changes. Formerly polarised and immobile epithelial cells which form cell junctions and cobblestone-like cell sheets undergo a transition into highly motile, elongated, mesenchymal cells lacking cell-to-cell adhesions. To explore how the proteome is affected during EMT we profiled protein expression and tracked cell biological markers in Madin-Darby kidney epithelial cells undergoing hepatocyte growth factor (HGF) induced EMT. We were able to identify and quantify over 4000 proteins by mass spectrometry. Enrichment analysis of this revealed that expression of proteins associated with the ubiquitination machinery was induced, whereas expression of proteins regulating apoptotic pathways was suppressed. We show that both the mammalian Hippo/MST2 and the ISG15 pathways are regulated at the protein level by ubiquitin ligases. Inhibition of the Hippo pathway by overexpression of either ITCH or A-Raf promotes HGF-induced EMT. Conversely, ISG15 over-expression is sufficient to induce cell scattering and an elongated morphology without external stimuli. Thus, we demonstrate for the first time that the Hippo/MST2 and ISG15 pathways are regulated during growth-factor induced EMT.

INTRODUCTION

Epithelial to Mesenchymal Transition (EMT) is a process that transforms polarised epithelial cells with tight cell to cell junctions into detached, motile fibroblast-like mesenchymal cells (1). EMT is an essential and tightly controlled developmental process that plays a fundamental role during embryogenesis, wound healing and tissue repair (2). Pathological EMT has been implicated in organ fibrosis (3) and in tumour development (4, 5). During cancer progression cancerous epithelial cells are thought to undergo EMT and acquire stem cell-like properties, allowing individual cells to bud off the tumour mass, invade the surrounding tissue, intravasate into lymph and blood vessels and finally metastasise by forming distant, secondary tumours (6). EMT can be triggered by a plethora of growth-factors, prominently TGFβ, HGF, EGF, Wnt and Hedgehog which have been shown to initiate and promote EMT in cancer, organ fibrosis and embryonic development (7). As diverse as the extra-cellular input can be, the downstream pathways which drive the transition are remarkably conserved across developmental and pathological EMT. Signalling networks are thought to converge on a few transcription factors chiefly Snail, Slug, Twist1, Twist2, Zeb1 and Zeb2/Sip1 (8). These transcription factors orchestrate the down-regulation of the epithelial junction proteins E-cadherin, occludins, claudins and connexins, and the up-regulation of the mesenchymal proteins N-cadherin, vimentin, α-smooth muscle actin, fibronectin, specific myosin isoforms and MMP. The transcriptional suppressor Snail has been reported to be the master switch as it potently suppresses the expression if the epithelial junction protein E-cadherin, with its, alone being sufficient to induce EMT in many systems (9). More recently, it has emerged that the transcriptional programme is not the whole picture. For example, alternative splicing and ubiquitin-mediated degradation of the small GTPases Rac and RhoA are induced during EMT.

RhoA is ubiquitinated by Smurf, an E3-ligase, and subsequently degraded through the proteasome (10). On the other hand, EMT-induced MMP expression triggers the expression of an alternatively spliced Rac1 (11). The induced protein, Rac1b, fails to bind to its regulatory inhibitor, RhoGDI and is therefore intrinsically over-active. Correspondingly, the shift in the balance of these two key cell motility drivers induces the migratory phenotype archetypal for mesenchymal cells.

Thanks to the widespread availability of sequencing and RNA-arrays additional layers of EMT regulation by microRNAs and alternative splicing events are starting to be revealed (12, 13). Although powerful, these approaches are only a surrogate to what happens at the protein level as they cannot capture changes to protein stability and the subsequent regulation of expression levels at the systems-level. Advances in mass spectrometry hardware and analysis software have made protein expression quantification, down to the level of weakly expressed signalling proteins, technically feasible (14). Therefore, in order to close this gap we profiled how protein expression is affected over the course of growth-factor induced. This body of work reveals novel facets of EMT, which have not been captured by or have been overlooked in previous RNA-based approaches.

EXPERIMENTAL SECTION

Cell culture: MDCK cells were seeded onto a 6-well plate at a density of 1 x 10^5 cells per well and incubated overnight. Cells were stimulated with 20 ng/mL of HGF in 5% DMEM over a time-course of 0, 1, 2, 4, 8, 24 hours, and lysed in 1% SDS Tris Saline buffer, sonicated and clarified by centrifugation.

NuPAGE and Western Blotting: Cell lysates were boiled in LDS-Sample buffer containing 100mM DTT, separated on a 4-12% gradient NuPage-gel (Invitrogen) and blotted on PVDF membranes (Whatman) according to the manufacturer's recommendations. The following primary antibodies were used α-tubulin, A-Raf, LATS1, RASSF1, Vimentin (Santa Cruz), E-cadherin, ITCH (BD Biosciences), SLUG, SNAIL (NEB), GAPDH (Millipore), HERC6 (abcam); secondary antibodies were from Cell Signaling.

MDCK Cell Scatter Assay: MDCK cells (Clone 3B5) were seeded out at a density of 3×10^3 per 6-well dish in 10% DMEM and incubated for 48 hours. When approximately 8-12 cells per colony were visible, the 10% serum DMEM was removed from the cells and replaced with DMEM containing 5% serum and 20 ng/mL HGF. Cells were incubated over a time-course of 24, 8, 4, 2, 1 and 0 hours in triplicate, before being fixed with 4% (v/v) PFA in PBS. After fixation cells were permeabilised with 0.1% Triton X-100 in PBS at room temperature for 5 minutes. Cell nuclei and F-actin were stained by adding DAPI and Alexa Fluor® Green Phalloidin stain according to the manufacturer's recommendation. The cells were washed and covered with PBS before High Content Screening (HCS). Images were acquired with Olympus Scan^R Automated Image Acquisition Software on a Scan^R IX81 microscope (Olympus) with a UPLSAPO 10x/0.40 NA objective (Olympus) and 1344 x 1024 resolution cooled CCD camera. Standard excitation and emission filter sets were used. A total of 81 sub-positions per well were acquired.

Image Analysis: Acquired images were analysed using CellProfiler (Broad Institute) and Columbus (Perkin Elmer) cell analysis software to determine cell spreading and changes in nuclear and cell size and morphology. A Cell Profiler pipeline was set up to identify primary objects, nuclei, using a typical diameter between 15 and 40 pixels, Otsu Global two-class

thresholding and clumped objects distinguished by intensity. Distances between the nuclei centroids and the centroid of the first and second nearest neighbouring nucleus were measured in pixels. A minimum of 800 cells were analysed per replicate. Means per well were calculated and standard deviations determined using means of three replicates. Images were further analysed by the Columbus analysis software. Nuclei and cytoplasm was segmented using the DAPI and FITC/Alexa Fluor 488 channels respectively. Border cells were discarded from the subsequent analysis protocol. The size, roundness and intensities of nuclei were measured. The cell and cytoplasm size and roundness were also determined.

Immunofluorescence: MDCK cells were seeded, treated, fixed and permeabilised as described above. The cells were incubated overnight in a 1:200 dilution of E-cadherin antibody in TBS-T. Cells were washed twice and incubated with an Alexa488-labelled anti-rabbit antibody (Invitrogen) for 1hour. Cells were imaged either on a Zeiss epi-fluorescent or Zeiss confocal laser scanning microscope (LSM 510 META). Images were acquired following excitation with 364 and 488 nm lasers followed by 385-470 and 505-530 nm BP (Band Pass) filters for DAPI and Alexa488 respectively with a Plan-Neoflur 20x/0.5 NA objective.

Oris Cell Migration Assays: 20,000 cells were plated in the cell migration system (Oris cell migration assembly kit, Platypus Technologies) according to the manufacturer's instructions until they reached confluency after 24 hours. The medium was then exchanged with DMEM containing 5% FCS and HGF (20ng/ml) before the stoppers were removed and cells were incubated to permit migration for 24 hours. As control, stoppers remained in place in the pre-migration reference wells until the time of the assay readout. Cells were stained with calcein AM (4 μM) for 30 minutes before measuring cell migration using fluorescence microscopy and the

ImageJ software. Comparison of migration was assessed using Student's t-test. P-values of less than 0.05 were considered significant.

Cell Adhesion Assay: 24-well dishes were coated with rat-tail collagen I, bovine fibronectin or vitronectin overnight at 4°C. Plates were blocked with 0.5% BSA in DMEM for 30 min. MDCK cells either treated with HGF for 24 hours, or left untreated, were trypsinised. After addition of 0.2% Soybean Trypsin Inhibitor cells were diluted in 0.5% BSA in DMEM, and 10,000 cells per well were seeded into a 24-well plate and allowed to adhere. After 30 minutes the plates were washed with PBS and shaken for 30 seconds at 400 rpm in order to wash-off loose cells. Cell were fixed with 4% PFA for 10 min, washed with PBS and stained with Crystal Violet (5mg/ml in 2% Ethanol/Water) for 10 minutes. Plates were washed with water, and the stain was dissolved with 100µl of 2% SDS. 50µl of the eluted stain solution was pipetted into a 96-well plate and absorbance was read at 550nm. Absorbance values were normalised by subtracting a control (unspecific binding to plastic).

Luciferase Reporter Assay: MDCK cells were seeded into 24-well dishes and transfected with a YAP/TAZ luciferase reporter (15). 24 hours post transfection the cells were stimulated with HGF as indicated, co-incubated with either DMSO or 10 µM PP2 (Tocris), a specific Src-family kinase inhibitor. After stimulation the cells were washed with PBS, and lysed on the plates with 80 µl of Luciferase Assay Buffer (Promega) including one freeze-thaw cycle. 20 µl of the lysate were pipetted into a white-rimmed 96-well plate, mixed with 100 µl of Luciferase Substrate Buffer (Promega). Luciferase was measured on a SynergyHT BioTek micro-plate reader and normalised by protein content.

Stable Isotope Labelling with Amino Acids in Cell Culture (SILAC): MDCK cells were cultured for at least seven days in light, medium and heavy SILAC media (Dundee Cell products) composed of DMEM media supplemented with 10% (v/v) FBS dialysed in-house. 2 x 10^4 cells were seeded in 60 mm tissue culture dishes and stimulated 24 hours post-seeding with 20 ng/mL HGF. The cells were lysed in 100 µL of 1% SDS-buffer, sonicated and cleared by centrifugation. The protein concentration was determined by a BCA-assay (Pierce). Heavy, medium and light SILAC lysates were mixed 1:1:1 and in-solution digested with trypsin using the FASP-protocol(16). Yield was determined by 280nm absorbance on a Nanodrop spectrophotometer. 60 µg of peptides were fractionated using strong-anion exchange chromatography as described(16).

Liquid Chromatography-Tandem Mass Spectrometry (LC-MS/MS): The tryptic peptide samples were separated on a Nanoflow Ultimate 3000 LC (Thermo) coupled online to a Q-Exactive mass spectrometer (Thermo). The self-packed HPLC C18-reversed phase column used was 10cm long, 75 µm inner diameter, packed with a ReproSIL AQ C18 1.8µm resin. The complex peptide mixtures were loaded at 600nL/min onto the column. The peptides were eluted at a constant flow rate of 250nL/min over a period of 40 or 120 min with a multi-segment linear gradient of 2-35% buffer B (98% Acetonitrile and 0.1% formic acid) in positive ion mode. A data-dependent automatic "top 12" method was employed with a survey scan (MS) in the mass range of a mass-to-charge ratio (m/z) of 350-1600 which selected the twelve most intense ions for collision induced fragmentation and acquisition of tandem mass spectra. An ion selection limit of 8300 was applied for the counts and selected ions were dynamically excluded for the next 40 seconds. The selection limit was chosen as it delivered most peptide identifications in a pilot experiment (Data not shown). The raw mass spectrometric data files from LC-MS/MS were analysed using

MaxQuant (Version 1.2) (17). Trypsin was selected as enzyme, first search and fragmentation spectra were searched with 20 ppm mass accuracy, recalibrated *in silico* and subsequently searched with the parent ion mass accuracy reduced to 6 ppm (18). Fixed modifications were carbamylation of cysteines, variable modifications were methionine oxidation and protein N-terminal acetylation. We allowed for two missed cleavages. The data were searched against a canine (CANFA) database (Version 0612, 25542 entries), a reversed canine (CANFA) database and a contaminant data base (152 entries). A false discovery rate (FDR) of 0.01 at the peptide and protein level. FDR was estimated by searching a reversed and forward database(19).

Data Analysis: Protein expression ratios were calculated by MaxQuant as published (20). Ratios were inverted in order to have the Medium label as the denominator and the Low and High labels as the numerator. Average ratios, standard deviation, standard error were derived from the protein ratios calculated by MaxQuant across three biological replicates. If we were able to quantify the protein ratio only in one replicate this value was chosen. Pair-wise comparisons and p-value calculation between untreated and individual timepoints post-HGF were done by Student's t-Test. P-values of less than 0.05 were deemed to be significant.

Enrichment Analysis: DAVID (Database for Annotation, Visualization and Integrated Discovery) Bioinformatics Resources 6.7 was utilised for Gene Ontology analysis (21). On the DAVID homepage: http://david.abcc.ncifcrf.gov/, the Functional Annotation tool was selected. Gene lists were uploaded and matched to human gene-names. Enrichment analysis and functional clustering of GOTERM_BP_FAT terms were done against a human database as background. A "high stringency" classification cut-off, corresponding to a kappa value of 0.85, was selected. Enrichment analysis with 10 gene-lists extracted at random from our quantified dataset consistently sported lower enrichment scores (data not shown).

ISG15 Cloning: Total cellular RNA was isolated from MDCK cells by RNeasy minikit (Qiagen). 1 μg of total RNA was reverse transcribed by using Oligo dT Primers (Invitrogen) using Quantitect reverse transcription Kit (Qiagen). Canine ISGF15 with stop codon (525bp) was amplified by real-time PCR using the following primers: 5'-ATGCTGGAGCCTACAGCCAT-3' and 3'-TCAGCACTGCCCTCCTGGT-5'. Platinum Taq DNA Polymerase High Fidelity (Invitrogen) was used. The Taq-amplified PCR product was gel-purified using QIAquick PCR purification kit (Qiagen) and cloned into the pCR™8/GW/TOPOR entry vector following the manufacturer's guidelines. Plasmids were sequenced to confirm the presence and orientation of the insert by using the GW1 and GW2 primers included in the kit. Once characterized, one clone was transferred into a puromycin –resistant derivative of TAPE5-N destination vector (22) using LR Gateway® Technology.

RESULTS AND DISCUSSION

Quantitative proteome and cell biological analysis of growth-factor induced EMT

HGF has been reported to potently induce EMT in MDCK cells within a matter of hours(23). After 24h the majority of the cells in the population have completed EMT. Although of canine origin, the speed and consistency of the HGF-induced transition makes MDCK cells an attractive and reliable model system for studying EMT. This transition can be tracked by monitoring cell scattering of sparsely seeded cell colonies. Although widely used, this approach has two major disadvantages. Firstly, monitoring of colony scattering can be laborious and subjective as this is done by visually inspecting the state of individual colonies. Secondly, scattering captures only one of the aspects of EMT, namely the induction of cell migration and the dissolution of cell junctions. Other salient parameters such as changes to the morphology and cell spreading are not

assayed. In order to address these shortcomings we decided to implement an unbiased, automated approach which would allow us to exactly quantify cell migration, cell spreading and changes in cellular morphology at the single cell level. Enhanced cell migration or scattering can be measured by assaying the distance between neighbouring nuclei; cell spreading can be monitored by measuring the size of the cytoplasm of individual cells; and finally, changes in cell morphology can be interpreted from changes in the roundness of individual cells. In order to monitor these three values accurately, individual cells had to be segmented, including identification of the nuclear and cytoplasm areas. To accomplish this, we stained fixed cells with a combination of DAPI, which stains the nucleus, and Alexa488-tagged phalloidin which stains the actin cytoskeleton (Fig 1 A). Cells were imaged using an automated screening microscope and analysed using an image analysis software suite (Columbus) as described in the Methods section. As readouts we chose the size of the cytoplasm, the roundness of the cells and the first and second nearest neighbour inter-nuclear distance. We assayed how these readouts change in MDCK cells over a 24 hour long time-course of HGF stimulation in three replicates (Fig 1 B). As expected, HGF stimulation increased the inter-nuclear distance indicating enhanced scattering, and the cytoplasmic spread. Conversely, cell roundness decreased consistent with cytoskeletal changes occurring during EMT. The assay was found to be robust, and we decided to use it for validating potential regulators of EMT which we planned to identify using proteomic profiling.

We observed that the cells started spreading within one hour of HGF treatment and that after 24 hours a significant proportion of the cell population had lost cell-to-cell adhesions and had adopted an elongated, mesenchymal phenotype (Fig 1 A&B, Fig S1). Thus, using mass spectrometry (MS)-based quantitative proteomics we profiled protein expression over 24 hours,

starting at 1 hour post-treatment. Metabolic, isotopic labelling, such as SILAC, is an established method for quantifying changes of protein expression in cell culture derived samples. SILAC allows to the identification of subtle changes of less than 20% in expression level (24). Therefore, we used a triple-SILAC approach to profile time-dependent HGF-induced expression changes. Samples were mixed immediately post-lysis, limiting experimental variability. Each of our SILAC-sets included an untreated standard condition, allowing us to compare time-points of individual experiments. Additionally, we permuted light and heavy labelled samples in three biological replicates to limit systemic labelling-dependent errors (Figs 1C&D). MDCK cells were lysed in an SDS-buffer and sonicated to ensure full lysis and solubilisation of membrane and DNA-binding proteins. The samples were processed and digested with trypsin using the FASP protocol(16). In order to enhance the proteome coverage, tryptic peptides were further fractionated on strong anion exchange (SAX) columns and then analysed by LC-MS/MS.

This approach allowed us to identify over 4400 proteins with over 40000 peptides of which 4100 were quantified at least at two time-points (Table S1). Of these, 626 proteins were increased or decreased in abundance of at least 1.5 fold with a p-value of <0.05 in at least one time-point (Fig 2A and Table S2). As expected, the number of significant changes increased over the time-course, with 124 proteins changing after 1 hour and over 400 regulated at the 24 hour time-point (Fig 2B).

HGF alters cell adhesion by regulating integrins and cadherins

Gene-ontology enrichment analysis for all 626 regulated proteins showed enrichment of proteins functioning in cell cycle, adhesion, apoptosis and metabolic regulators (Table S3). In agreement with previous studies we observed a switch in the abundance of integrins (25) (Fig 2C).

Integrins α2, 3 and β1, 4 (ITGA2,3 ITGB1,4) were rapidly induced, reaching their maximum expression within one hour. In addition, the stem-cell and invasive tumour marker, integrin α6 (ITGA6)(26), was strongly induced throughout the HGF treatment, peaking at 24 hours. Conversely, the expression of integrins αv and β3 (ITGAV, ITGB3) was only slightly reduced 24 hours post-treatment. Taken together, this suggests that HGF does not induce the expression of vitronectin and fibronectin receptors (αvβ3) and consequently should not affect or even reduce cell adhesion to either ligand. On the other hand, integrins able to bind collagen and laminin (α2β1, α6β4, α3β1, α3β4 and α6β1) increased, which should facilitate adhesion to either. To experimentally verify these predictions we performed *in vitro* cell adhesion assays. MDCK cells, which were stimulated with HGF for 24 hours or left untreated, were seeded into collagen, fibronectin or vitronectin coated dishes. Cell-to-matrix adhesion was interrupted after 30 minutes by washing, and the cells remaining adherent were fixed, stained and counted colourimetrically. MDCK cells adhered stronger to collagen in comparison to fibronectin and vitronectin. The adherence to collagen was further and significantly increased when cells had been treated with HGF (Fig 2D). Conversely, fibronectin and vitronectin binding was slightly reduced after HGF treatment, in line with the expectations we derived from expression profiling. Similarly to what we observed in the integrin family, we detected an isoform specific regulation of cadherins (Fig 2E). Unexpectedly, the epithelial marker E-cadherin (CDH1) did not decrease significantly even after 24 hours of HGF stimulation (Fig S1A). This finding is counterintuitive, as the silencing of E-cadherin, in concurrence with the loss of cell junctions, is seen as a marker of mesenchymal transition(27). On the other hand, another classical marker of mesenchymal cells, vimentin, increases over the time-course and reaches a plateau 8 hours post-treatment (Fig S1A), suggesting that MDCK cells undergo EMT. Cellular E-Cadherin is in a persistent state of flux,

being internalised through endocytosis, degraded in lysosomes or shuttled back to the membrane through the trans-Golgi network (28). It is therefore plausible that E-cadherin may be removed from cell junctions and re-localise to a different cellular compartment, resulting in loss of membrane-bound E-cadherin without altering the total cellular abundance. Thus, we visualised E-cadherin in cells at various timepoints of HGF treatment by immunofluorescence. In untreated cells, E-cadherin localised specifically at cellular junctions. Within one hour of HGF treatment cells that had started to spread and were losing cell-to-cell adhesions, showed a remarkable shift of membrane-bound to perinuclear E-cadherin (Suppl. Fig S1B). Fully mesenchymal cells seemed to have internalised most of the cellular pool of E-cadherin to the perinuclear compartment (Fig 2F). This observation supports the hypothesis that the suppression of E-cadherin expression is not a prerequisite for EMT, but rather a shift away from the cell junctions appears to be sufficient. Indeed it has been recently reported that cancers expressing perinuclear E-cadherin are particularly aggressive in terms of metastasis and invasion (29), suggesting that these cancers have undergone EMT. There is further *in vivo* evidence that loss of E-cadherin is not necessary for EMT in breast cancers(30). In contrast to E-cadherin, P-cadherins (CDH3), and LI –cadherin (CDH 17) were strongly induced. P-Cadherin, whose expression has been linked to invasion and poor prognosis in breast cancer (31), was rapidly and transiently induced, peaking at 1 hour. On the other hand LI-Cadherin was elevated in a sustained fashion, reaching its plateau at 4 hours. Expectedly, the classical mesenchymal marker vimentin linearly increased, peaking at 24 hours. In addition to expression changes of integrins and cadherins, we identified potential positive feedback and autocrine loops. We detected a rapid induction of Sonic Hedgehog as well as of cMET, the HGF receptor (Fig 2G). This is indicative of a Hedgehog autocrine loop as well as of a mechanism to sustain HGF-signalling by increasing overall receptor levels.

Dynamic protein expression changes during HGF-induced EMT

As EMT is a highly orchestrated and dynamic process, we wanted to extract more information out of the time-course data in order to identify groups of proteins which were regulated in transient waves. For this purpose we normalised the data, and clustered the significantly changing proteins according to their temporal profiles (Fig 3A&B). Increasing the number of clusters beyond six yielded very small clusters, thus we chose to cluster the proteins into six individual clusters. The majority of proteins increased or decreased linearly in a time-dependent fashion. Cluster II and IV are examples of these. Gene-ontology enrichment analysis was performed on each cluster and (Table S4) revealed that proteins regulating the cell cycle, cell migration, integrin signalling, ubiquitination and transcription increased over 24 hours of HGF treatment. In contrast, metabolic enzymes, pro-apoptotic and transcriptional suppressors decreased over the same period. Cluster V contained proteins whose expression declined sharply within one hour and remained suppressed for up to 24 hours. This cluster was enriched for metabolic enzymes and pro-apoptotic as well as transcriptional regulators. Furthermore, three clusters contained proteins which were elevated only transiently. Cluster VI proteins were upregulated only at the earliest, one hour time-point; it was enriched for proteins involved in the DNA-damage response and protein transport. Cluster III also contained early responders encompassing proteins upregulated at 1-4 hours. In line with the previous cluster, DNA damage and endocytosis regulators were enriched. A further cluster of delayed, transient responders was grouped in Cluster I. This cluster was again enriched for endocytic and vesicle transport proteins. In summary, this analysis suggests that HGF induces a transient DNA-repair response as well as transiently regulates endocytosis and vesicle transport. This early and transient upregulation of endocytosis is interesting in light of our observation that E-cadherin is rapidly

internalised in response to HGF. It is conceivable that the rapid re-localisation of E-cadherin is driven by an increase in endocytic activity. Further, we found that a proportion of expression changes are detectable already after 1 hour, which is well before the 4-8 hour timeframe when major changes in cell biological markers become pronounced.

The sustained up-regulation of ubiquitination pathways in concert with the decrease of pro-apoptotic proteins in clusters II, IV and V led us to further hypothesise that pro-apoptotic pathways are modulated by ubiquitination-dependent degradation during HGF stimulation and that this regulation enhances EMT.

HGF regulates the Hippo-pathway

To test this hypothesis, we analysed the dataset for pro-apoptotic pathways, which were specifically regulated by HGF and which in turn can be inhibited by ubiquitination. Pathway analysis revealed that proteins, which regulate or function in the mammalian Hippo/MST2 pathway, were enriched in the induced/suppressed dataset (Fig 4A). The core pathway consists of the kinases MST1/2 which phosphorylate LATS, which in turn phosphorylates YAP1, a transcriptional co-regulator that mediates many of the diverse pathway outputs (32). These include proliferation when YAP binds to TEAD transcription factors (33-35) and apoptosis when YAP interacts with p73(36-38). Potent, activators of the pathway, such as PLK1 (39) and Aurora kinase B (40) were strongly induced. In addition to upstream activators, the expression of several proteins regulating the pathway at the level of MST2 and LATS1 were altered. Interestingly, we found that the protein levels of the ubiquitin-ligase ITCH increased almost twofold within 24 hours (Fig 4B). ITCH has been reported to ubiquitinate the tumour suppressor LATS1 leading to its degradation(41, 42). In addition to this potential ubiquitin-regulated mechanism of LATS1

downregulation, we detected that A-Raf, a potent inhibitor of MST2(43, 44), was elevated. These data support the hypothesis that the upstream part of the pathway is hyperactivated only for the pro-apoptotic signal to be blocked at the level of the kinases MST and LATS. A similar mode of MST pathway regulation has recently been observed in EGF stimulated cells, where MST2 activity was activated but its interaction with LATS blocked, resulting in the disruption of apoptotic signalling (45). Interestingly, the MST2- pathway has recently emerged as a potential inducer of EMT and metastasis(46). In over-expression or depletion experiments several members of the pathway have been shown to induce mesenchymal-like phenotypes in MCF10a cells(42, 47-49). Thus far, no evidence has been presented confirming that the pathway is endogenously regulated during growth-factor induced EMT. Our data suggest that the pathway is regulated upon HGF stimulation and involved in promoting EMT. Therefore, we decided to extend the coverage of protein quantification by Western blotting. Furthermore, to ascertain whether suppressing the pathway enhances EMT, we decided to perform functional assays.

Analogous to our proteomic screen, we seeded MDCK cells and stimulated them with HGF over a 24 hour period. After lysis we analysed the protein expression of classical EMT markers and of members of the mammalian Hippo/MST2 pathway by Western blotting (Fig 5A). The transcription factors Snail and Slug, both of which have been established to be EMT master-switches, were rapidly induced within one to two hours. Unexpectedly, the induction was not sustained beyond 8 hours of HGF treatment, suggesting that both Snail and Slug are not required to maintain the phenotype after the transition has been initiated. In agreement with our previous quantification, both A-Raf and ITCH were induced to levels which were roughly double that of the basal expression. ITCH induction was somewhat faster, becoming visible at 2 hours, whereas A-Raf levels were only elevated beyond 4 hours. ITCH has been shown to reduce LATS1 protein

levels and we could verify an inverse correlation between ITCH and LATS1 expression, confirming this inhibitory link. The proteomic data showed that the upstream activators, Aurora kinase B and PLK1were increased. In addition, we found by Western blotting that RASSF1, a potent inducer of Hippo-signalling, was induced, peaking at 4 hours. In conclusion, we could confirm the observed protein level changes by alternative means and could also demonstrate that there is an inverse relationship between ITCH and LATS1 expression.

The Hippo/MST2 pathway has been recently reported to be activated downstream of receptor-tyrosine kinases (45). Therefore, we examined whether HGF may also be able to activate YAP1 transcription downstream of the cMET receptor. In order to assay YAP1 transcriptional activity we transfected a luciferase reporter construct (15) transiently into MDCK cells and stimulated them with HGF over a time-course (Fig. 5B). We detected a rapid induction of luciferase activity, peaking at 2-4 hours after HGF stimulation. The luciferase activity subsequently declined to basal levels over 24 hours, confirming that YAP1 is activated in a transient fashion by HGF. There are currently no specific small molecule inhibitors of the MST/LATS pathway. However, as HGF activates Src (50), and Src can activate the MST pathway (51) and also directly phosphorylate YAP (52), we hypothesised that Src-family kinases may be key signal-transducers downstream of cMET and upstream of YAP. We therefore tested the effects of Src inhibition on HGF induced YAP transcriptional activity. The Src-family kinase inhibitor (PP2) completely abrogated the induction of YAP1-driven luciferase transcription (Fig. 5C). Interestingly, over 24 hours the levels of luciferase activity declined to 12.5% of the basal levels. Taken together, these data suggest that Src activity is not only necessary for HGF induction of YAP transcriptional activity, but also for the maintenance of basic YAP function.

ITCH and ARaf positively contribute towards growth-factor induced EMT

After having confirmed that the protein abundance of several components of the MST/LATS pathway are regulated during HGF-induced EMT, we wanted to establish whether there was a causal relationship, and which aspects of EMT are influenced. Therefore, we overexpressed ITCH or A-Raf to levels comparable to their induction observable post-HGF stimulation. For this purpose we produced a cell line, which stably expressed A-Raf-eGFP at a level similar to endogenous A-Raf protein, thus mimicking the ca. twofold upregulation during EMT (Fig 6A). Similarly, ITCH levels were increased two-fold by transient transfection (Fig 7A). In both situations we quantified changes in cell roundness, size of the cytoplasm and cell scattering induced by HGF stimulation over 24 hours using high content screening microscopy and the analysis methods developed in Fig. 1. A-Raf over-expression had no effect on scattering as neither nearest first or second neighbour distances differed significantly. In terms of cell shape and cell size there was a mild yet significant acceleration of the increase of the cytoplasmic spread and decrease of cell roundness (Fig 6B). This acceleration was only significant at the early time-points. By 24 hours both populations were indistinguishable from each other. Although A-Raf over-expression accelerated some phenotypic features of EMT in MDCK cells, the enhancement was only marginal and partial. Cell scattering is consistent with random, non-directed migration. Thus, we examined whether A-Raf expression enhanced directed migration of HGF-treated MDCK cells. To this end we performed Oris cell migration assays, a variant of scratch assays, which measures cell migration directed into a wound. Cells were stimulated by HGF and wound closure was measured after 24 hours (Fig 6C). Whereas random cell migration was not affected by A-Raf overexpression, directed migration was increased significantly (Fig. 6D), thus confirming that A-Raf overexpression enhances cell motility induced by HGF in MDCK cells despite only marginally affecting EMT.

Similar to A-Raf, ITCH overexpression did not affect untreated cells, but had transient as well as sustained effects on scattering, cell spreading and cell morphology upon HGF stimulation (Fig 7B). Overexpression of ITCH significantly accelerated the acquisition of all mesenchymal cell traits measured. Cell roundness was decreased and the cytoplasmic spread was significantly increased at the 8 hour time-point. Cell scattering on the other hand increased at the endpoint, resulting in significantly greater inter-nuclear distances after 24 hour HGF stimulation. In summary, these results suggest that the inhibition of the pathway at the level of MST2 and LATS1 is insufficient to trigger EMT, but enhances EMT induced by HGF.

ISG15 and ISGylation are induced during HGF-driven EMT

Aside from the induction of ITCH, we detected that protein levels of the small, ubiquitin-like protein ISG15 were rapidly elevated (Figs 8A). We further detected that the E3-ligase HERC6, which has been reported to be the enzyme responsible for ISGylation of proteins(53), was simultaneously induced (Table S1). By contrast, the related ubiquitin-specific ligases HERC4 and UBE2L6 were not induced at the protein level. These observations lead us to hypothesise that HGF may induce the ISGylation of proteins during EMT. Interestingly, elevated ISGylation has been linked to cytoskeletal changes, increased cell motility (54), and has been proposed to be a marker for aggressive, high-grade cancers of the breast and bladder (55). We blotted lysates of MDCK cells treated with HGF and detected ISG15 and adducts with an ISG15-specific antibody.

Unconjugated, free ISG15 was detected as a faint band running just above the 15 kDa marker, which increased upon HGF stimulation (Fig. 8B). We further observed that ISG15-positive bands (at 37 kDa and 75 kDa) as well as HERC6 increased after HGF treatment (Fig. 8C), thus,

confirming that protein ISGylation, ISG15 and the expression of its E3-ligase, HERC6, increased in response to HGF stimulation.

In order to test if ISG15 positively regulates EMT, we over-expressed TAP-tagged (SF-TAP(22, 56)) canine ISG15 in MCDK cells. Over-expression of ISG15 induced a moderate increase of cellular ISGylation. In addition, we were able to detect the unbound as well as the bound Flag-tagged ISG15 in the lysates (Fig. 8D). Surprisingly, ISG15 expression was sufficient to induce changes to the cell morphology (Fig. 8E). The cells were more spread out, had lost cell-to-cell adhesion, polarity and adopted a fibroblast-like mesenchymal phenotype. Having observed that ISG15 over-expression was sufficient to induce scattering in MDCK cells we quantified inter-nuclear distances, cell spread and cell shape by using high content screening microscopy in cells growing in 10% FCS. In confirmation of our observation we observed that the ISG15 over-expressing population was more scattered and spread and adopted a more elongated phenotype (Fig. 8F). Thus, in contrast to A-Raf and ITCH, ISG15 over-expression induces changes in cell morphology and behaviour which are typical for EMT. On the other hand, other EMT markers, such as directed migration, were not significantly affected by ISG15 over-expression under basal conditions (Data not shown). Therefore, ISG15 over-expression on its own appears not to be sufficient to induce the full transition.

CONCLUSIONS

In the current study we set out to quantify how the proteome changes when epithelial MDCK cells transition into a mesenchymal phenotype. We hypothesised that those proteins, the expression of which drives the transition, would experience significant expression changes.

Although this is likely to be valid, over 600 proteins fulfilled this criterion. In order to filter this list and to increase the likelihood of identifying drivers, we assumed that significant expression changes would cluster and highlight pivotal pathways. Using complementary methodologies of proteomics we demonstrated that the expression of crucial inhibitors and effectors of the mammalian Hippo/MST2 pathway are regulated at the protein level. Several members of the pathway have been shown to be induced or suppressed in metastatic and aggressive cancers, for example YAP and TEAD are overexpressed in sarcomas(57). Conversely, LATS1 knock-out mice develop soft-tissue sarcoma(58), demonstrating that the deregulation of the pathway induces mesenchymal tumours. Subsequently, it was shown that the inhibition of upstream activators of the pathway and LATS itself are able to mimic YAP overexpression(47). Here, we demonstrate that the pathway is indeed regulated in response to EMT inducing growth-factors, suggesting that the MST/LATS pathway is a physiological mediator of this process. The detailed results appear to be more nuanced. When EMT is triggered by HGF, the MST/LATS pathway is inhibited at the level of MST2 and LATS, whereas the upstream activators RASSF1, PLK1, Aurora kinase B are induced. This is in contrast with previous findings which demonstrate that knock-down of some of these activators can initiate EMT(47, 48). However, our data further suggest that the induction of the upstream activators is nullified by the inhibition of LATS and MST2 by ITCH or A-Raf, respectively. This decoupling may indicate that the upstream activators function in other pathways in EMT, or that it is specifically the pro-apoptotic function of MST/LATS that is shut down during EMT. The general downregulation of proteins associated with apoptosis (Table S2) makes the latter interpretation plausible, although these possibilities are not mutually exclusive.

YAP itself has a dual role and can function either as a tumour suppressor or an oncoprotein depending on the context. When associated with p73, YAP strongly induces apoptosis(36, 59), whereas it can function as pro-survival and proliferation signal when in complex with TEAD(46, 60, 61). Pro-apoptotic YAP signalling requires MST2 and LATS signalling, whereas its association with TEAD can proceed independent of either(15). Interestingly, the activation of YAP1 by HGF is transient and peaks before ITCH and A-Raf are induced. Two likely scenarios are possible. Either, HGF induces YAP1 transcriptional activity independent of the MST/LATS pathway, possibly through a Src-dependent mechanism. Alternatively, the MST/LATS pathway could induce rather than suppress YAP and TEAD activation. The transient nature of the activation would thus be directly resulting from the suppression of MST and LATS1 caused by the increase in A-Raf and ITCH expression. Both situations have founding in the literature. Activation of Yes, a Src-family kinase, has been shown to bind, phosphorylate and regulate YAP1 sub-cellular localisation(60, 62). Further, in mammalian systems, the MST2/Lats1 axis activates YAP1 transcriptional activity(59). Which one of these scenarios is valid, should be determined by follow-up experiments.

Additionally, we discovered that the small ubiquitin-like protein ISG15 as a regulator of EMT. This finding is exciting, as ISG15 signalling has been predominately studied in the context of interferon signalling and not in the framework of EMT or cancer progression (63). It is now emerging that signalling regulated by ISG15 is much more complex and broader than initially thought. ISG15 is emerging as a potential novel oncoprotein. Oncogenic K-RasV12 and ISG15 appear to be interlocked into a mutual positive feed-back loop and knock-down of ISG15 or its E2-ligase, UbcH8, partially reverts EMT in the highly metastatic and mesenchymal breast cancer cell line MDA-MB-231(64). Exogenous expression of K-RasV12 in NIH-3T3 cells enhances

cellular ISGylation. Conversely, knock-down of ISG15 expression reduces protein levels of mutant K-Ras in MDA-MB-231 cells. As MDCK cells do not express mutant Ras isoforms, it is unlikely that this positive feedback-loop is the driver of EMT in this cell line. Future experiments will have to reveal which pathways and nodes are regulated by ISGylation in MDCK cells and we are currently mapping the interactome in these cells.

Quite surprisingly many of the proteins we detected as regulated by HGF have been reported to be pro-invasive or are markers of metastasis. Aside from the above examples, inhibition of αvβ3(65, 66), as well as expression of Sonic Hedgehog (67) and cMET (68) have been shown to drive invasion. As MDCK cells are not tumour derived and of canine origin this suggests that pathways and nodes are conserved across species and the individual sub-types of EMT. Thus, we can confirm that MDCK cells are a useful model system, which replicates pathological and physiological processes with accuracy.

SUPPORTING INFORMATION

Supplementary Figure S1

Supplementary Table S1; All protein and peptide information (two panels)

Supplementary Table S2; Proteins significantly changing ($p<0.05$) (two panels)

Supplementary Table S3; GO-enrichment clusters of significantly changed proteins (Table S2)

Supplementary Table S4; GO-enrichment of clusters I-VI (6 panels)

This material is available free of charge via the Internet at http://pubs.acs.org

Author Contributions

The manuscript was written through contributions of all authors. All authors have given approval to the final version of the manuscript.

ACKNOWLEDGMENT

We would like to thank Prof. Dmitri Scholz from UCD Conway Imaging Facility as well as the Mass Spectrometry Facility for hosting the equipment. We also acknowledge Dr Tapesh Santra for normalising the expression ratios, Dr Fabio Carrozzino for sending us MDCK II cells clone 3B5. Science Foundation Ireland (SFI) for funding under Grant No. 06/CE/B1129. The JCS lab is supported by a Principal Investigator (PI) award (kata) from SFI.

ABBREVIATIONS

DAPI: 4',6-diamidino-2-phenylindole; DMEM: Dulbecco's Modified Eagle Medium; DTT: Dithiothreitol; eGFP: enhanced green fluorescent protein; EGF: Epithelial Growth Factor; EMT: Epithelial to Mesenchymal Transition; HCS: High Content Screening; HERC: HECT domain and RCC1-like domain-containing protein; HGF: Hepatocyte Growth Factor; ISG15: Interferon-induced 17 kDa protein; ITCH: E3 ubiquitin-protein ligase Itchy homolog; LATS: Large Tumour Suppressor; MDCK: Madin-Darby canine kidney cells; MMP: Matrix-Metalloproteinase; MST: Mammalian Ste20-like protein; PFA: Para-formaldehyde; RASSF1: Ras association domain-containing protein 1; RhoGDI: Rho GDP-dissociation inhibitor; SILAC: Stable isotope labeling by amino acids in cell culture; TAP: Tandem-Affinity-Purification; TGFβ: Transforming growth factor beta; YAP: Yes-associated protein;

REFERENCES

(1) Kalluri, R.; Weinberg, R. A., The basics of epithelial-mesenchymal transition. *The Journal of clinical investigation* **2009,** 119, (6), 1420-8.

(2) Martin, P.; Parkhurst, S. M., Parallels between tissue repair and embryo morphogenesis. *Development* **2004,** 131, (13), 3021-34.

(3) Zeisberg, M.; Yang, C.; Martino, M.; Duncan, M. B.; Rieder, F.; Tanjore, H.; Kalluri, R., Fibroblasts derive from hepatocytes in liver fibrosis via epithelial to mesenchymal transition. *The Journal of biological chemistry* **2007,** 282, (32), 23337-47.

(4) Voulgari, A.; Pintzas, A., Epithelial-mesenchymal transition in cancer metastasis: mechanisms, markers and strategies to overcome drug resistance in the clinic. *Biochimica et biophysica acta* **2009,** 1796, (2), 75-90.

(5) Mani, S. A.; Guo, W.; Liao, M. J.; Eaton, E. N.; Ayyanan, A.; Zhou, A. Y.; Brooks, M.; Reinhard, F.; Zhang, C. C.; Shipitsin, M.; Campbell, L. L.; Polyak, K.; Brisken, C.; Yang, J.; Weinberg, R. A., The epithelial-mesenchymal transition generates cells with properties of stem cells. *Cell* **2008,** 133, (4), 704-15.

(6) Huber, M. A.; Kraut, N.; Beug, H., Molecular requirements for epithelial-mesenchymal transition during tumor progression. *Current opinion in cell biology* **2005,** 17, (5), 548-58.

(7) Thiery, J. P.; Sleeman, J. P., Complex networks orchestrate epithelial-mesenchymal transitions. *Nature reviews. Molecular cell biology* **2006,** 7, (2), 131-42.

(8) Voutsadakis, I. A., The ubiquitin-proteasome system and signal transduction pathways regulating Epithelial Mesenchymal transition of cancer. *Journal of biomedical science* **2012,** 19, 67.

(9) Onder, T. T.; Gupta, P. B.; Mani, S. A.; Yang, J.; Lander, E. S.; Weinberg, R. A., Loss of E-cadherin promotes metastasis via multiple downstream transcriptional pathways. *Cancer research* **2008,** 68, (10), 3645-54.

(10) Wang, H. R.; Zhang, Y.; Ozdamar, B.; Ogunjimi, A. A.; Alexandrova, E.; Thomsen, G. H.; Wrana, J. L., Regulation of cell polarity and protrusion formation by targeting RhoA for degradation. *Science* **2003,** 302, (5651), 1775-9.

(11) Radisky, D. C.; Levy, D. D.; Littlepage, L. E.; Liu, H.; Nelson, C. M.; Fata, J. E.; Leake, D.; Godden, E. L.; Albertson, D. G.; Nieto, M. A.; Werb, Z.; Bissell, M. J., Rac1b and reactive oxygen species mediate MMP-3-induced EMT and genomic instability. *Nature* **2005,** 436, (7047), 123-7.

(12) D'Amato, N. C.; Howe, E. N.; Richer, J. K., MicroRNA regulation of epithelial plasticity in cancer. *Cancer letters* **2012**.

(13) Shapiro, I. M.; Cheng, A. W.; Flytzanis, N. C.; Balsamo, M.; Condeelis, J. S.; Oktay, M. H.; Burge, C. B.; Gertler, F. B., An EMT-driven alternative splicing program occurs in human breast cancer and modulates cellular phenotype. *PLoS genetics* **2011,** 7, (8), e1002218.

(14) Geiger, T.; Wehner, A.; Schaab, C.; Cox, J.; Mann, M., Comparative proteomic analysis of eleven common cell lines reveals ubiquitous but varying expression of most proteins. *Molecular & cellular proteomics : MCP* **2012,** 11, (3), M111 014050.

(15) Dupont, S.; Morsut, L.; Aragona, M.; Enzo, E.; Giulitti, S.; Cordenonsi, M.; Zanconato, F.; Le Digabel, J.; Forcato, M.; Bicciato, S.; Elvassore, N.; Piccolo, S., Role of YAP/TAZ in mechanotransduction. *Nature* **2011,** 474, (7350), 179-83.

(16) Wisniewski, J. R.; Zougman, A.; Mann, M., Combination of FASP and StageTip-based fractionation allows in-depth analysis of the hippocampal membrane proteome. *Journal of proteome research* **2009,** 8, (12), 5674-8.

(17) Cox, J.; Mann, M., MaxQuant enables high peptide identification rates, individualized p.p.b.-range mass accuracies and proteome-wide protein quantification. *Nature biotechnology* **2008,** 26, (12), 1367-72.

(18) Cox, J.; Michalski, A.; Mann, M., Software lock mass by two-dimensional minimization of peptide mass errors. *Journal of the American Society for Mass Spectrometry* **2011,** 22, (8), 1373-80.

(19) Cox, J.; Neuhauser, N.; Michalski, A.; Scheltema, R. A.; Olsen, J. V.; Mann, M., Andromeda: a peptide search engine integrated into the MaxQuant environment. *Journal of proteome research* **2011,** 10, (4), 1794-805.

(20) Cox, J.; Matic, I.; Hilger, M.; Nagaraj, N.; Selbach, M.; Olsen, J. V.; Mann, M., A practical guide to the MaxQuant computational platform for SILAC-based quantitative proteomics. *Nature protocols* **2009,** 4, (5), 698-705.

(21) Huang da, W.; Sherman, B. T.; Lempicki, R. A., Systematic and integrative analysis of large gene lists using DAVID bioinformatics resources. *Nature protocols* **2009,** 4, (1), 44-57.

(22) von Thun, A.; Birtwistle, M.; Kalna, G.; Grindlay, J.; Strachan, D.; Kolch, W.; von Kriegsheim, A.; Norman, J. C., ERK2 drives tumour cell migration in three-dimensional microenvironments by suppressing expression of Rab17 and liprin-beta2. *Journal of cell science* **2012,** 125, (Pt 6), 1465-77.

(23) Ridley, A. J.; Comoglio, P. M.; Hall, A., Regulation of scatter factor/hepatocyte growth factor responses by Ras, Rac, and Rho in MDCK cells. *Molecular and cellular biology* **1995,** 15, (2), 1110-22.

(24) Mann, M., Functional and quantitative proteomics using SILAC. *Nature reviews. Molecular cell biology* **2006,** 7, (12), 952-8.

(25) Chen, Y. S.; Mathias, R. A.; Mathivanan, S.; Kapp, E. A.; Moritz, R. L.; Zhu, H. J.; Simpson, R. J., Proteomics profiling of Madin-Darby canine kidney plasma membranes reveals Wnt-5a involvement during oncogenic H-Ras/TGF-beta-mediated epithelial-mesenchymal transition. *Molecular & cellular proteomics : MCP* **2011,** 10, (2), M110 001131.

(26) Lathia, J. D.; Gallagher, J.; Heddleston, J. M.; Wang, J.; Eyler, C. E.; Macswords, J.; Wu, Q.; Vasanji, A.; McLendon, R. E.; Hjelmeland, A. B.; Rich, J. N., Integrin alpha 6 regulates glioblastoma stem cells. *Cell stem cell* **2010,** 6, (5), 421-32.

(27) Cano, A.; Perez-Moreno, M. A.; Rodrigo, I.; Locascio, A.; Blanco, M. J.; del Barrio, M. G.; Portillo, F.; Nieto, M. A., The transcription factor snail controls epithelial-mesenchymal transitions by repressing E-cadherin expression. *Nature cell biology* **2000,** 2, (2), 76-83.

(28) Bryant, D. M.; Stow, J. L., The ins and outs of E-cadherin trafficking. *Trends in cell biology* **2004,** 14, (8), 427-34.

(29) Harigopal, M.; Shin, S. J.; Murray, M. P.; Tickoo, S. K.; Brogi, E.; Rosen, P. P., Aberrant E-cadherin staining patterns in invasive mammary carcinoma. *World journal of surgical oncology* **2005,** 3, 73.

(30) Hollestelle, A.; Peeters, J. K.; Smid, M.; Timmermans, M.; Verhoog, L. C.; Westenend, P. J.; Heine, A. A.; Chan, A.; Sieuwerts, A. M.; Wiemer, E. A.; Klijn, J. G.; van der Spek, P. J.; Foekens, J. A.; Schutte, M.; den Bakker, M. A.; Martens, J. W., Loss of E-cadherin is not a necessity for epithelial to mesenchymal transition in human breast cancer. *Breast cancer research and treatment* **2013**.

(31) Paredes, J.; Correia, A. L.; Ribeiro, A. S.; Albergaria, A.; Milanezi, F.; Schmitt, F. C., P-cadherin expression in breast cancer: a review. *Breast cancer research : BCR* **2007,** 9, (5), 214.

(32) Pan, D., The hippo signaling pathway in development and cancer. *Developmental cell* **2010,** 19, (4), 491-505.

(33) Zhang, L.; Ren, F.; Zhang, Q.; Chen, Y.; Wang, B.; Jiang, J., The TEAD/TEF family of transcription factor Scalloped mediates Hippo signaling in organ size control. *Developmental cell* **2008,** 14, (3), 377-87.

(34) Wu, S.; Liu, Y.; Zheng, Y.; Dong, J.; Pan, D., The TEAD/TEF family protein Scalloped mediates transcriptional output of the Hippo growth-regulatory pathway. *Developmental cell* **2008,** 14, (3), 388-98.

(35) Zhao, B.; Ye, X.; Yu, J.; Li, L.; Li, W.; Li, S.; Lin, J. D.; Wang, C. Y.; Chinnaiyan, A. M.; Lai, Z. C.; Guan, K. L., TEAD mediates YAP-dependent gene induction and growth control. *Genes & development* **2008,** 22, (14), 1962-71.

(36) Matallanas, D.; Romano, D.; Yee, K.; Meissl, K.; Kucerova, L.; Piazzolla, D.; Baccarini, M.; Vass, J. K.; Kolch, W.; O'Neill, E., RASSF1A elicits apoptosis through an MST2 pathway directing proapoptotic transcription by the p73 tumor suppressor protein. *Molecular cell* **2007,** 27, (6), 962-75.

(37) Strano, S.; Monti, O.; Pediconi, N.; Baccarini, A.; Fontemaggi, G.; Lapi, E.; Mantovani, F.; Damalas, A.; Citro, G.; Sacchi, A.; Del Sal, G.; Levrero, M.; Blandino, G., The transcriptional coactivator Yes-associated protein drives p73 gene-target specificity in response to DNA Damage. *Molecular cell* **2005,** 18, (4), 447-59.

(38) Yee, K. S.; Grochola, L.; Hamilton, G.; Grawenda, A.; Bond, E. E.; Taubert, H.; Wurl, P.; Bond, G. L.; O'Neill, E., A RASSF1A polymorphism restricts p53/p73 activation and associates with poor survival and accelerated age of onset of soft tissue sarcoma. *Cancer research* **2012,** 72, (9), 2206-17.

(39) Mardin, B. R.; Agircan, F. G.; Lange, C.; Schiebel, E., Plk1 controls the Nek2A-PP1gamma antagonism in centrosome disjunction. *Current biology : CB* **2011,** 21, (13), 1145-51.

(40) Yabuta, N.; Mukai, S.; Okada, N.; Aylon, Y.; Nojima, H., The tumor suppressor Lats2 is pivotal in Aurora A and Aurora B signaling during mitosis. *Cell cycle* **2011,** 10, (16), 2724-36.

(41) Ho, K. C.; Zhou, Z.; She, Y. M.; Chun, A.; Cyr, T. D.; Yang, X., Itch E3 ubiquitin ligase regulates large tumor suppressor 1 stability [corrected]. *Proceedings of the National Academy of Sciences of the United States of America* **2011,** 108, (12), 4870-5.

(42) Salah, Z.; Melino, G.; Aqeilan, R. I., Negative regulation of the Hippo pathway by E3 ubiquitin ligase ITCH is sufficient to promote tumorigenicity. *Cancer research* **2011,** 71, (5), 2010-20.

(43) Matallanas, D.; Birtwistle, M.; Romano, D.; Zebisch, A.; Rauch, J.; von Kriegsheim, A.; Kolch, W., Raf family kinases: old dogs have learned new tricks. *Genes & cancer* **2011,** 2, (3), 232-60.

(44) Rauch, J.; O'Neill, E.; Mack, B.; Matthias, C.; Munz, M.; Kolch, W.; Gires, O., Heterogeneous nuclear ribonucleoprotein H blocks MST2-mediated apoptosis in cancer cells by regulating A-Raf transcription. *Cancer research* **2010,** 70, (4), 1679-88.

(45) Romano, D.; Maccario, H.; Doherty, C.; Quinn, N. P.; Kolch, W.; Matallanas, D., The differential effects of wildtype and mutated K-Ras on MST2 signalling are determined by K-Ras activation kinetics. *Molecular and cellular biology* **2013**.

(46) Lamar, J. M.; Stern, P.; Liu, H.; Schindler, J. W.; Jiang, Z. G.; Hynes, R. O., The Hippo pathway target, YAP, promotes metastasis through its TEAD-interaction domain. *Proceedings of the National Academy of Sciences of the United States of America* **2012,** 109, (37), E2441-50.

(47) Angus, L.; Moleirinho, S.; Herron, L.; Sinha, A.; Zhang, X.; Niestrata, M.; Dholakia, K.; Prystowsky, M. B.; Harvey, K. F.; Reynolds, P. A.; Gunn-Moore, F. J., Willin/FRMD6 expression activates the Hippo signaling pathway kinases in mammals and antagonizes oncogenic YAP. *Oncogene* **2012,** 31, (2), 238-50.

(48) Moleirinho, S.; Chang, N.; Sims, A. H.; Tilston-Lunel, A. M.; Angus, L.; Steele, A.; Boswell, V.; Barnett, S. C.; Ormandy, C.; Faratian, D.; Gunn-Moore, F. J.; Reynolds, P. A., KIBRA exhibits MST-independent functional regulation of the Hippo signaling pathway in mammals. *Oncogene* **2012**.

(49) Overholtzer, M.; Zhang, J.; Smolen, G. A.; Muir, B.; Li, W.; Sgroi, D. C.; Deng, C. X.; Brugge, J. S.; Haber, D. A., Transforming properties of YAP, a candidate oncogene on the chromosome 11q22 amplicon. *Proceedings of the National Academy of Sciences of the United States of America* **2006,** 103, (33), 12405-10.

(50) Organ, S. L.; Tsao, M. S., An overview of the c-MET signaling pathway. *Ther Adv Med Oncol* **2011,** 3, (1 Suppl), S7-S19.

(51) Wang, H. C.; Erikson, R. L., Activation of protein serine/threonine kinases p42, p63, and p87 in Rous sarcoma virus-transformed cells: signal transduction/transformation-dependent MBP kinases. *Molecular biology of the cell* **1992,** 3, (12), 1329-37.

(52) Liu, X.; Yang, N.; Figel, S. A.; Wilson, K. E.; Morrison, C. D.; Gelman, I. H.; Zhang, J., PTPN14 interacts with and negatively regulates the oncogenic function of YAP. *Oncogene* **2013,** 32, (10), 1266-73.

(53) Oudshoorn, D.; van Boheemen, S.; Sanchez-Aparicio, M. T.; Rajsbaum, R.; Garcia-Sastre, A.; Versteeg, G. A., HERC6 is the main E3 ligase for global ISG15 conjugation in mouse cells. *PloS one* **2012,** 7, (1), e29870.

(54) Hadjivasiliou, A., ISG15 implicated in cytoskeleton disruption and promotion of breast cancer. *Expert review of proteomics* **2012,** 9, (1), 7.

(55) Andersen, J. B.; Aaboe, M.; Borden, E. C.; Goloubeva, O. G.; Hassel, B. A.; Orntoft, T. F., Stage-associated overexpression of the ubiquitin-like protein, ISG15, in bladder cancer. *British journal of cancer* **2006,** 94, (10), 1465-71.

(56) Gloeckner, C. J.; Boldt, K.; Schumacher, A.; Roepman, R.; Ueffing, M., A novel tandem affinity purification strategy for the efficient isolation and characterisation of native protein complexes. *Proteomics* **2007,** 7, (23), 4228-34.

(57) Helias-Rodzewicz, Z.; Perot, G.; Chibon, F.; Ferreira, C.; Lagarde, P.; Terrier, P.; Coindre, J. M.; Aurias, A., YAP1 and VGLL3, encoding two cofactors of TEAD transcription factors, are amplified and overexpressed in a subset of soft tissue sarcomas. *Genes, chromosomes & cancer* **2010,** 49, (12), 1161-71.

(58) St John, M. A.; Tao, W.; Fei, X.; Fukumoto, R.; Carcangiu, M. L.; Brownstein, D. G.; Parlow, A. F.; McGrath, J.; Xu, T., Mice deficient of Lats1 develop soft-tissue sarcomas, ovarian tumours and pituitary dysfunction. *Nat Genet* **1999,** 21, (2), 182-6.

(59) Matallanas, D.; Romano, D.; Hamilton, G.; Kolch, W.; O'Neill, E., A Hippo in the ointment: MST signalling beyond the fly. *Cell cycle* **2008,** 7, (7), 879-84.

(60) Vassilev, A.; Kaneko, K. J.; Shu, H.; Zhao, Y.; DePamphilis, M. L., TEAD/TEF transcription factors utilize the activation domain of YAP65, a Src/Yes-associated protein localized in the cytoplasm. *Genes & development* **2001,** 15, (10), 1229-41.

(61) Chan, S. W.; Lim, C. J.; Loo, L. S.; Chong, Y. F.; Huang, C.; Hong, W., TEADs mediate nuclear retention of TAZ to promote oncogenic transformation. *The Journal of biological chemistry* **2009,** 284, (21), 14347-58.

(62) Mohler, P. J.; Kreda, S. M.; Boucher, R. C.; Sudol, M.; Stutts, M. J.; Milgram, S. L., Yes-associated protein 65 localizes p62(c-Yes) to the apical compartment of airway epithelia by association with EBP50. *The Journal of cell biology* **1999,** 147, (4), 879-90.

(63) Skaug, B.; Chen, Z. J., Emerging role of ISG15 in antiviral immunity. *Cell* **2010,** 143, (2), 187-90.

(64) Burks, J.; Reed, R. E.; Desai, S. D., ISGylation governs the oncogenic function of Ki-Ras in breast cancer. *Oncogene* **2014,** 33, (6), 794-803.

(65) Christoforides, C.; Rainero, E.; Brown, K. K.; Norman, J. C.; Toker, A., PKD controls alphavbeta3 integrin recycling and tumor cell invasive migration through its substrate Rabaptin-5. *Developmental cell* **2012,** 23, (3), 560-72.

(66) White, D. P.; Caswell, P. T.; Norman, J. C., alpha v beta3 and alpha5beta1 integrin recycling pathways dictate downstream Rho kinase signaling to regulate persistent cell migration. *The Journal of cell biology* **2007,** 177, (3), 515-25.

(67) Bailey, J. M.; Singh, P. K.; Hollingsworth, M. A., Cancer metastasis facilitated by developmental pathways: Sonic hedgehog, Notch, and bone morphogenic proteins. *Journal of cellular biochemistry* **2007,** 102, (4), 829-39.

(68) Birchmeier, C.; Birchmeier, W.; Gherardi, E.; Vande Woude, G. F., Met, metastasis, motility and more. *Nature reviews. Molecular cell biology* **2003,** 4, (12), 915-25.

FIGURE LEGENDS

Figure 1. EMT Quantification and Experimental Setup A. MDCK cells were treated with 20 ng/ml HGF for the indicated times. Post-treatment the cells were fixed, permeabilised and stained with Phalloidin and DAPI. Panel of representative images out of a total of 81 acquired per sample on the HCS microscope with a 10x objective, Phalloidin (green) and DAPI (blue) **B.**

Images obtained from (A) were analysed by the CellProfiler and Columbus software suites to determine intra-nuclear distances (nearest neighbour), roundness (1 being a perfect circle) and cytoplasmic size. Bar graphs represent the summary of three biological replicates. Error bars represent SD of the population averages **C.** Schematic of the proteomic workflow. SILAC-labelled cells were lysed, mixed, digested by filter aided sample preparation (FASP) and the peptides were subsequently fractionated by strong anion exchange chromatography. The six resulting fractions were analysed by LC-MS/MS. Peptides were identified by searching the raw data and statistical analysis with the MaxQuant software suite. The DAVID web-resource was used to do enrichment analysis **D.** Experimental design of how SILAC labelling was permuted across three biological replicates. Each biological replicate (Sets A-B) consists of two triple-SILAC subsets (1 and 2), in total the experiments contains 6 triple-SILAC experiments. The Medium (M) labelled sample is the 0 timepoint and is the standard to which the Light (L) and Heavy (H) labelled samples are compared. In order to avoid technical errors, the H- and L-labelled HGF treated samples are permuted across the biological replicates.

Figure 2. Results of proteomic profiling A. Clustering of proteins which significantly change at one time point at least (ttest p-value <0.05) as compared to untreated cells and have been quantified across all time points. Average protein ratios, as determined by MaxQuant, were log(2) transformed and clustered using the Perseus software suite. **B.** Bar graph representing the number of proteins which significantly change (ttest p-value <0.05) as compared to untreated at the specified time-points and across all times **C.** Average ratios across three replicates of Integrin-family proteins as compared to untreated cells. Error bars represent SEM of values across three replicates. If absent, the protein could be only quantified in one of the replicates **D.** Cell-matrix adhesion assay. Treated and untreated MDCK were seeded into 24-well dishes

coated as indicated, let to adhere for 30 minutes, fixed and stained with Crystal Violet. The dye was dissolved and absorption at 550nm was measured in a 96-well plate. Y-axis represents the normalised absorbance at 550nm, error bars are SD of three replicates p-values NS=Not significant *<0.05 ;***<0.001 **E.** Average ratios across three replicates of cadherin-family proteins and vimentin as compared to untreated cells. Error bars represent SEM of values across three replicates. If absent, the protein could be only quantified in one of the replicates **F.** Confocal image of E-cadherin and vimentin immuno-fluorescence. MDCK cell were treated with HGF accordingly, fixed and stained with DAPI (blue), an anti-E-Cadherin antibody detected with an anti-mouse Alexa488 labelled secondary antibody (green) and an anti-vimentin antibody detected with an anti-rabbit Alexa594 labelled secondary antibody (red). Scale bars represent 25µm **G.** Average ratios across three replicates of potential positive feedback regulators as compared to untreated cells. Error bars represent SEM of values across three replicates. If absent, the protein could be only quantified in one of the replicates

Figure 3. Clustering of temporal expression profiles Protein expression ratios were normalised and proteins which significantly change at one time point at least (ttest p-value <0.05) when compared to untreated cells and have been quantified across all time points (see Fig. 2A) were clustered into 6 groups **A.** Profiles of six individual clusters. Red is close to the mean, green is distant. x-Axis represent hours of HGF treatment. y-Axis are arbitrary units from -1 to 1 **B.** Heat-map of clustered, normalised and significantly changing proteins

Figure 4. The MST2/Hippo pathway is endogenously regulated upon HGF stimulation A. Pathway diagram of protein ratios (in black) 24 hours post HGF treatment vs. untreated detected in the proteomic screen **B.** Temporal profiles of Hippo pathway proteins identified which change significantly at one time-point at least (p-values <0.05) ;. The graph represents average

protein expression ratios across three replicates as compared to untreated cells Ratios. Error bars are SEM

Figure 5. Western Blot quantification of regulated Hippo/MST2 pathway proteins A. MDCK cells were treated as indicated, lysed, electro-blotted, detected with antibodies as indicated and imaged on a CCD-camera. Densitometric quantification was performed by ImageJ **B.** MDCK cells were transfected with a YAP/TAZ Luciferase reporter. The cells were subsequently stimulated with HGF as indicated. The cells were lysed and the expression of the reporter was quantified by measuring luciferase activity. The activity was corrected against protein concentration and normalised to the 0 h time-point. Graphs represent the average of four independent experiments, error bars are SEM. **C.** MDCK cells were transfected with a YAP/TAZ Luciferase reporter. The cells were subsequently incubated with the Src-family kinase inhibitor (PP2 10 μM) and stimulated with HGF as indicated. The cells were lysed and the expression of the reporter was quantified by measuring luciferase activity. The activity was corrected against protein concentration and normalised to the 0 h time-point. Graphs represent the average of three independent experiments, error bars are SEM

Figure 6. A-Raf expression enhances cell migration A. Western blot of MDCK cells stably expressing eGFP or eGFP-A-Raf, blotted with anti-A-Raf **B.** Quantification of cell scattering, roundness and cytoplasmic size of MDCK cells stably expressing eGFP (dark grey) or eGFP-A-Raf (light grey) as obtained from HCS. Bar graphs represent the summary of three biological replicates. Error bars represent SD of the population averages. **C.** MDCK cells were stably transfected with either A-Raf-EGFP or EGFP as control and plated in 96-well cell migration systems so they reached confluence within 24 hours. The stoppers were removed and cells incubated to permit migration for 24 hours. Representative images for both cell lines at start and

after 24 hours. **D.** Quantitation of the assay described in C. Shown as single values (black dots) from 20 wells and the mean (red line).

Figure 7. ITCH expression enhances EMT A. Western blot of MDCK cells transfected with an empty vector or Flag-ITCH, blotted with anti-ITCH and a Tubulin loading control. **B.** Quantification of cell scattering, roundness and cytoplasmic size of MDCK cells transfected with an empty vector (dark grey) or Flag-ITCH (light grey) as obtained from HCS. Bar graphs represent the summary of three biological replicates. Error bars represent SD of the population averages.

Figure 8. ISG15 pathway is activated and promotes EMT A. Temporal profiles of ISG15 and its ligases. **B.** Western Blot quantification of HERC6 and unbound ISG15 (15 kDa). MDCK cells were treated as indicated, lysed, electro-blotted, detected with antibodies as indicated and imaged on a CCD-camera. Densitometric quantification was performed by ImageJ. **C**. Western Blot quantification of HERC6 and endogenously ISGylated proteins (at 37 and 75 kDa).. MDCK cells were treated as indicated, lysed, electro-blotted, detected with antibodies as indicated and imaged on a CCD-camera. Densitometric quantification was performed by ImageJ. **D.** MDCK cells were transfected with either TAP-ISG15 or an empty vector as control and plated. The cells were fixed, permeabilised and stained with Phalloidin and DAPI. Panel of representative images out of a total of 81 acquired per sample on the HCS microscope. Phalloidin (green) and DAPI (blue) **E.** Western Blot quantification of ISG15 overexpression. MDCK cells were transfected with either TAP-ISG15 or an empty vector as control and lysed. ISGylated proteins and Flag-tagged proteins were detected after electro-blotting with anti-ISG15 (left section of composite figure) or anti-Flag (middle and right section of composite figure). **F.** Quantification of cell scattering, roundness and cytoplasmic size of MDCK cells transfected with an empty vector (dark grey) or

TAP-ISG15 (light grey) and growing in 10% FCS DMEM as obtained from HCS. Bar graphs represent the summary of three biological replicates. Error bars represent SD of the population averages.

Graphical Abstract

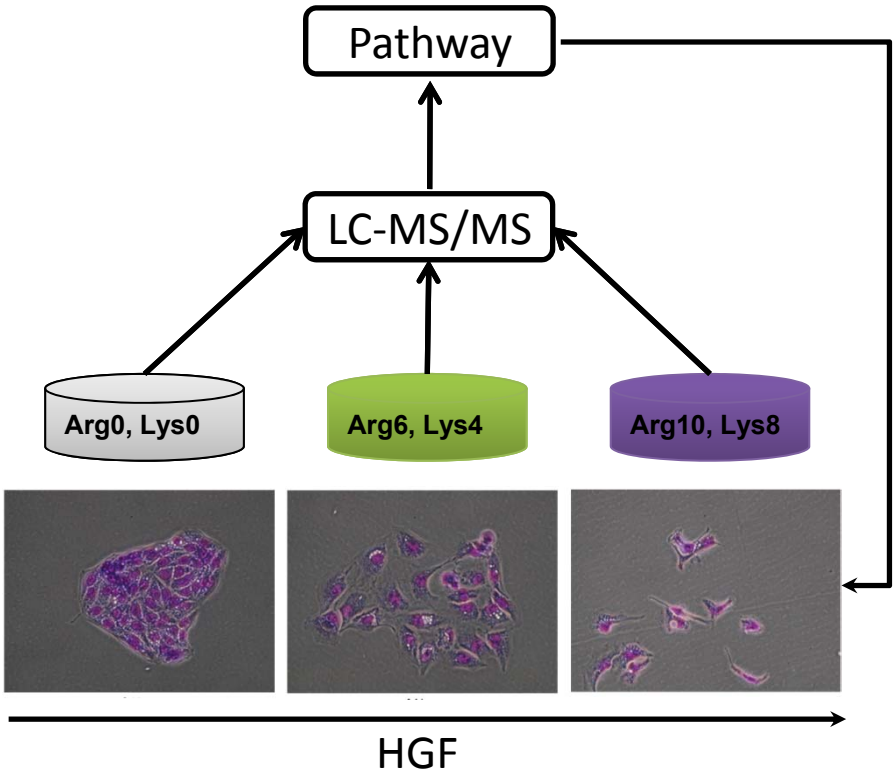

Figure 1

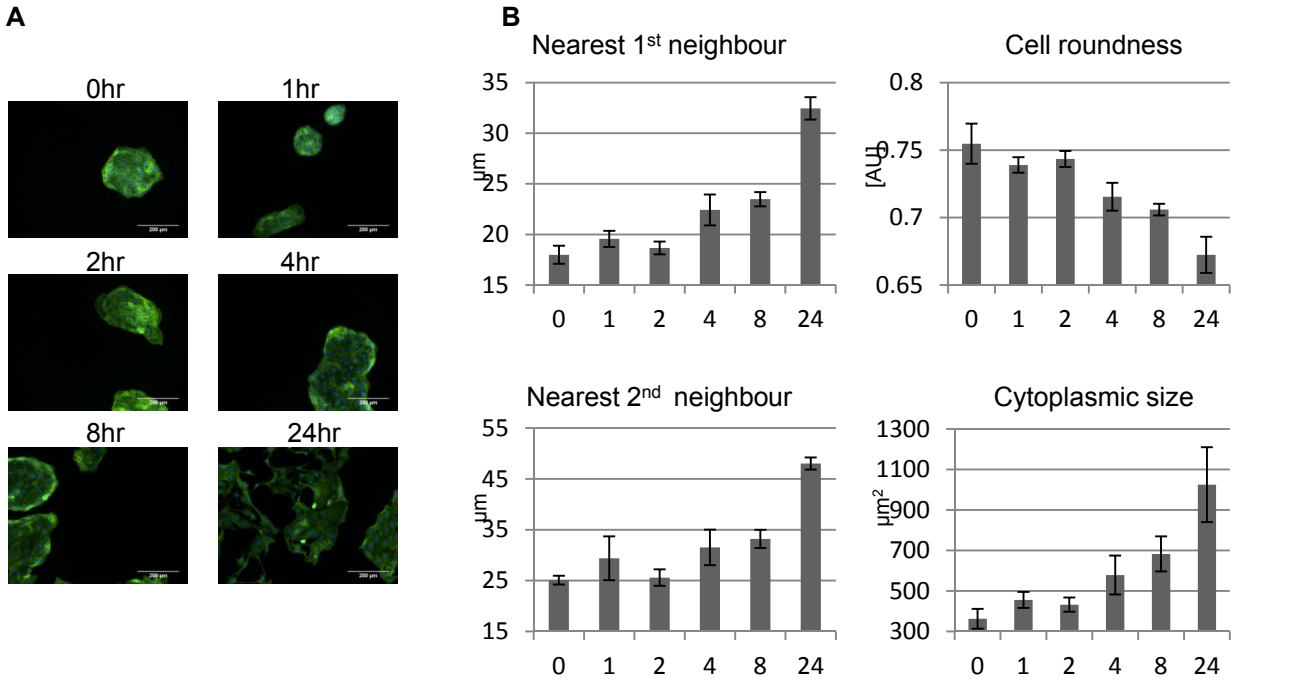

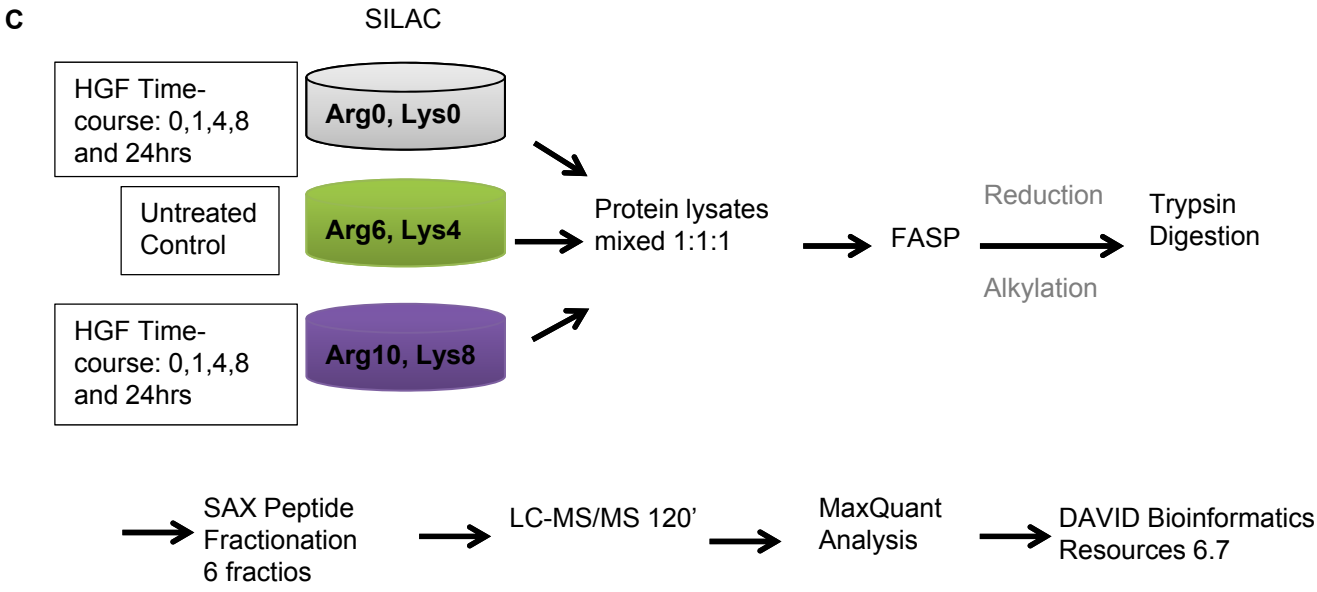

D

		SILAC- HGF Time-Course (hours)		
Set	***Subset***	**Arg0, Lys0 (L)**	**Arg6, Lys4 (M)**	**Arg10, Lys8 (H)**
A	*1*	1 *h HGF*	0 *h HGF*	4 *h HGF*
	2	8 *h HGF*	0 *h HGF*	24 *h HGF*
B	*1*	4 *h HGF*	0 *h HGF*	8 *h HGF*
	2	24 *h HGF*	0 *h HGF*	1 *h HGF*
C	*1*	1 *h HGF*	0 *h HGF*	8 *h HGF*
	2	24 *h HGF*	0 *h HGF*	4 *h HGF*

Figure 2

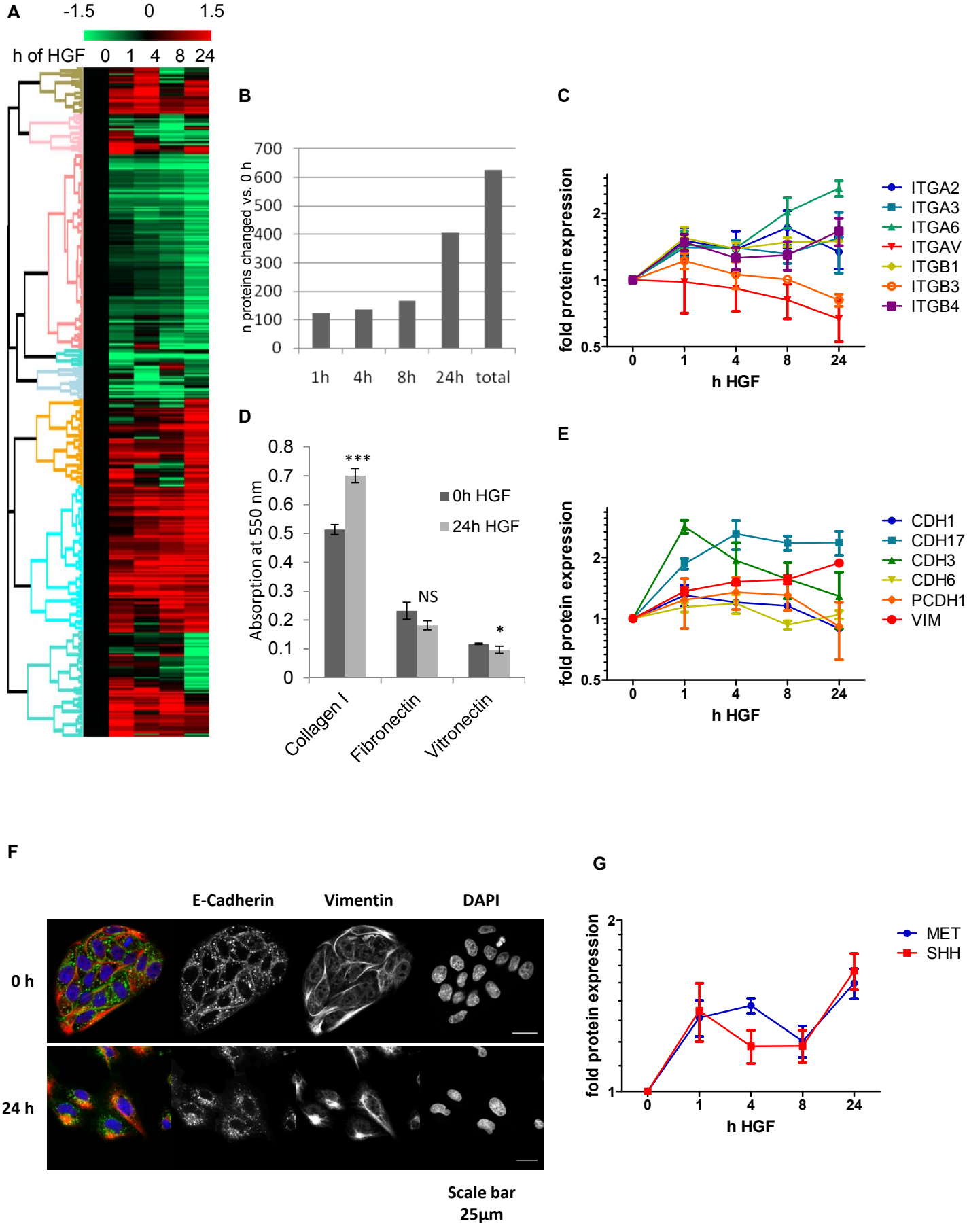
A
-1.5
0
1.5
h of HGF 0 1 4 8 24
B
n proteins changed vs. 0 h
700
600
500
400
300
200
100
0
1h
4h
8h
24h
total
C
fold protein expression
2
1
0.5
0
1
4
8
24
h HGF
ITGA2
ITGA3
ITGA6
ITGAV
ITGB1
ITGB3
ITGB4
D
Absorption at 550 nm
0.8
0.7
0.6
0.5
0.4
0.3
0.2
0.1
0
***
NS
*
0h HGF
24h HGF
Collagen I
Fibronectin
Vitronectin
E
fold protein expression
2
1
0.5
0
1
4
8
24
h HGF
CDH1
CDH17
CDH3
CDH6
PCDH1
VIM
F
E-Cadherin
Vimentin
DAPI
0 h
24 h
Scale bar
25µm
G
fold protein expression
2
1
0
1
4
8
24
h HGF
MET
SHH

Figure 3

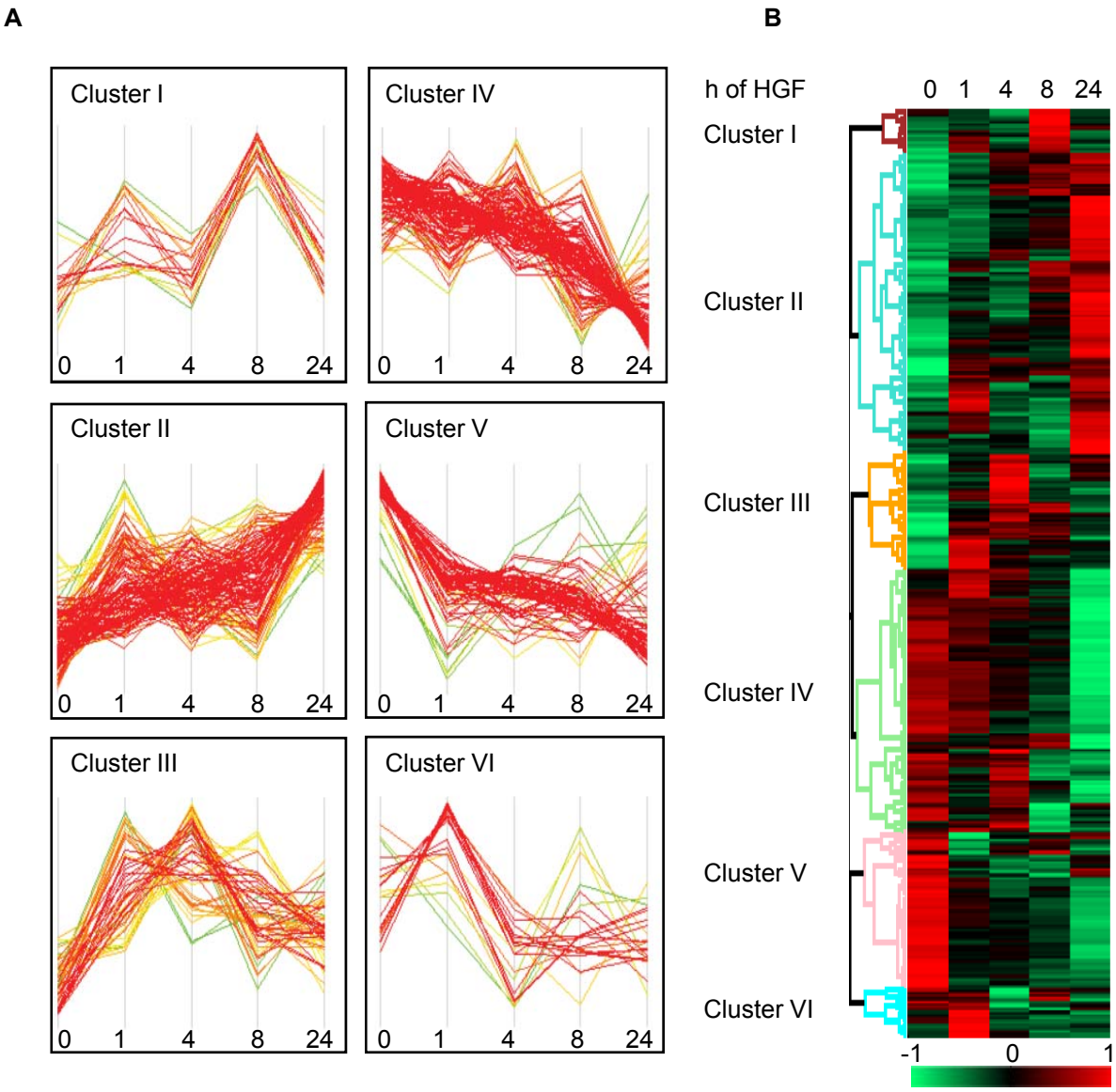
A
B
Cluster I
Cluster IV
Cluster II
Cluster V
Cluster III
Cluster VI
0 1 4 8 24
h of HGF
Cluster I
Cluster II
Cluster III
Cluster IV
Cluster V
Cluster VI
0 1 4 8 24
-1 0 1

Figure 4

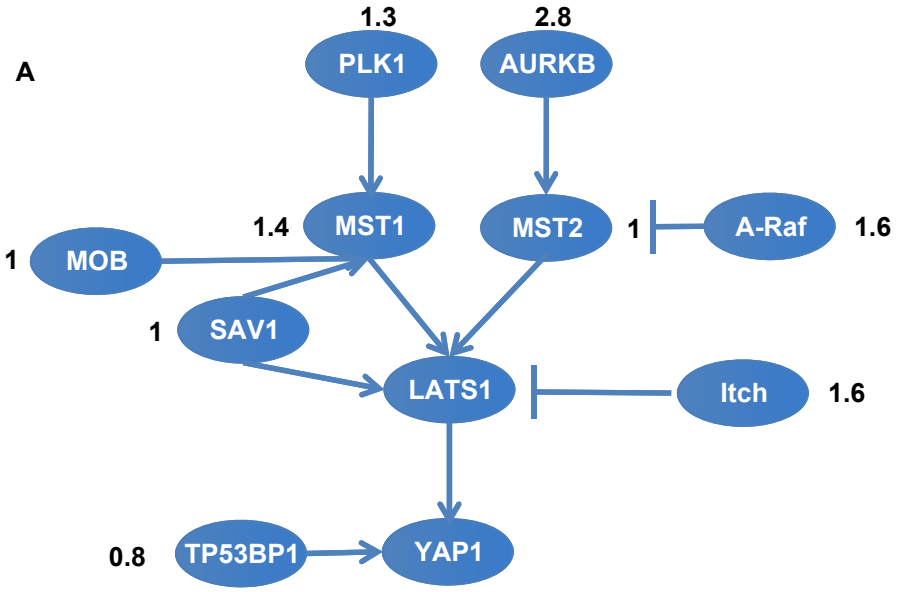
A
1.3
PLK1
2.8
AURKB
1.4
MST1
MST2
1
A-Raf
1.6
1
MOB
1
SAV1
LATS1
Itch
1.6
0.8
TP53BP1
YAP1

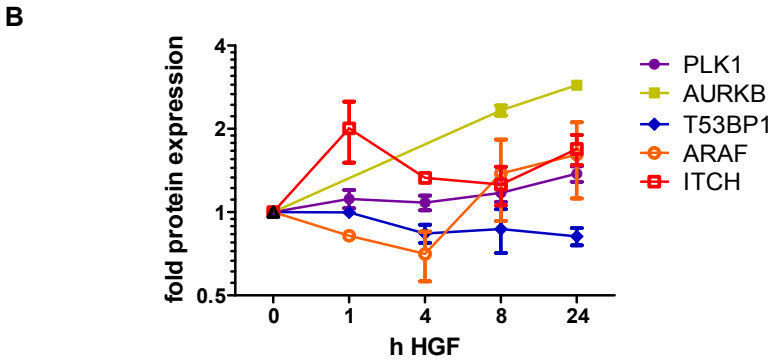
B
fold protein expression
4
2
1
0.5
0
1
4
8
24
h HGF
PLK1
AURKB
T53BP1
ARAF
ITCH

Figure 5

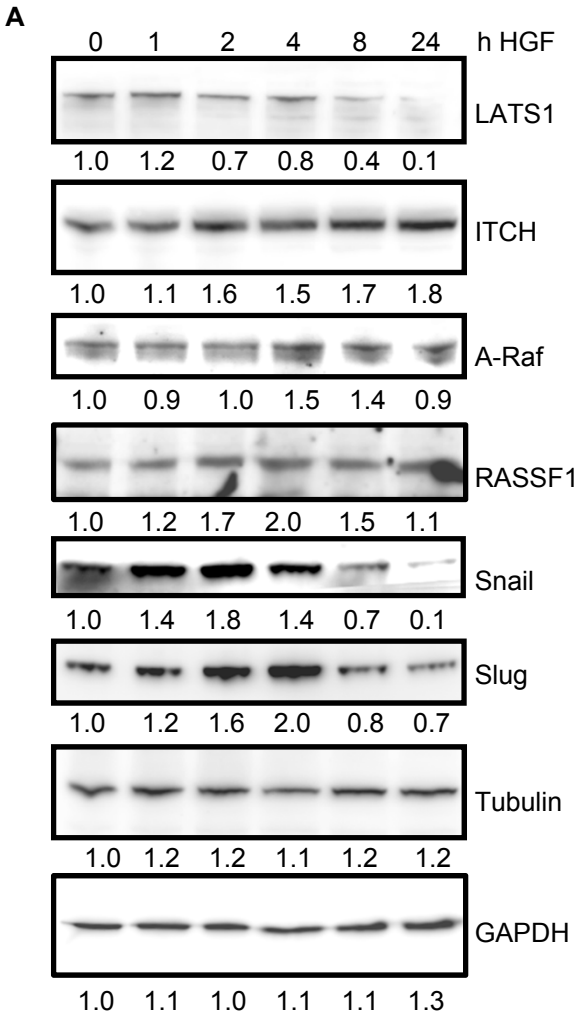
A
0 1 2 4 8 24 h HGF
LATS1
1.0 1.2 0.7 0.8 0.4 0.1
ITCH
1.0 1.1 1.6 1.5 1.7 1.8
A-Raf
1.0 0.9 1.0 1.5 1.4 0.9
RASSF1
1.0 1.2 1.7 2.0 1.5 1.1
Snail
1.0 1.4 1.8 1.4 0.7 0.1
Slug
1.0 1.2 1.6 2.0 0.8 0.7
Tubulin
1.0 1.2 1.2 1.1 1.2 1.2
GAPDH
1.0 1.1 1.0 1.1 1.1 1.3

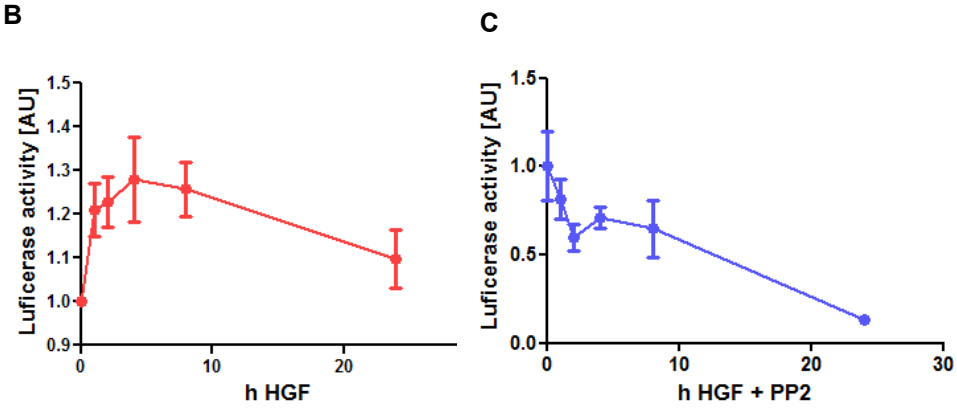
B
Luficerase activity [AU]
h HGF
C
Luficerase activity [AU]
h HGF + PP2

Figure 6

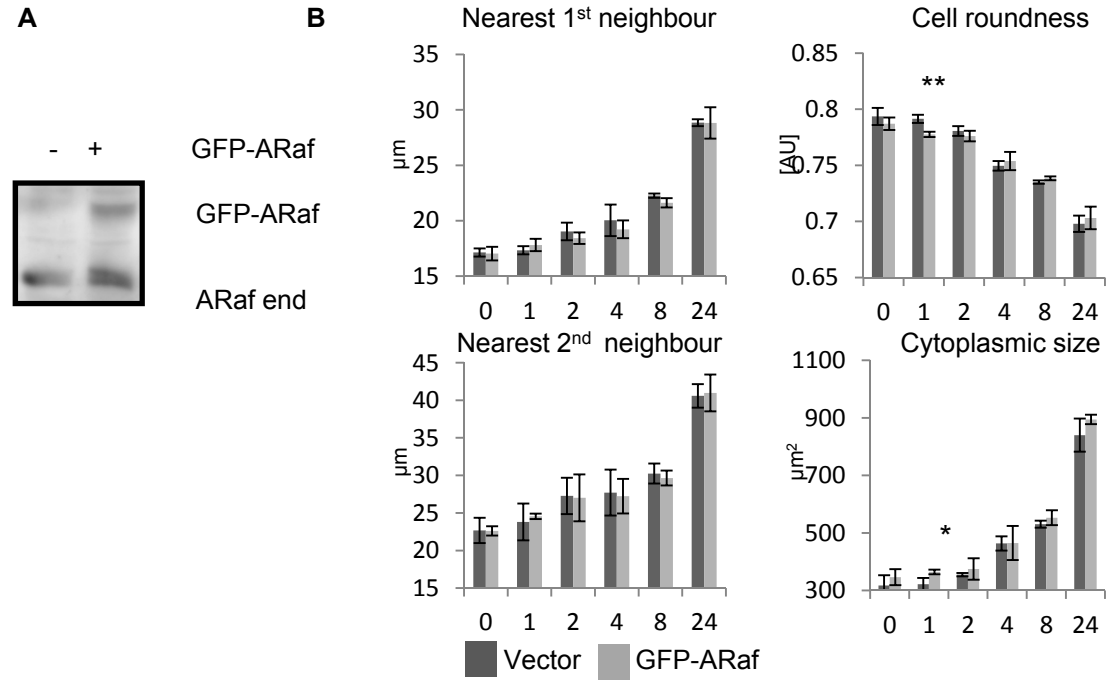
A
B
- +
GFP-ARaf
GFP-ARaf
ARaf end
Nearest 1st neighbour
Cell roundness
Nearest 2nd neighbour
Cytoplasmic size
µm
[AU]
µm²
0 1 2 4 8 24
Vector
GFP-ARaf

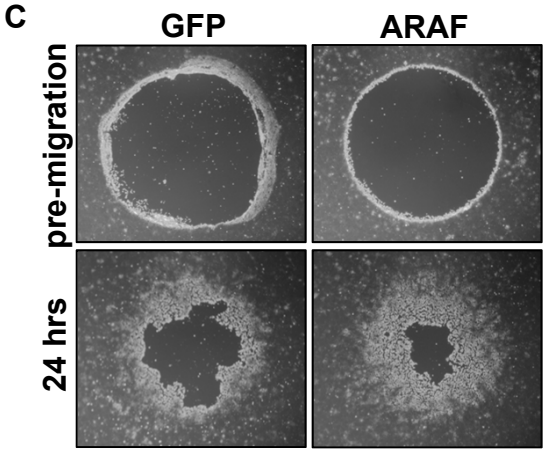
C
GFP
ARAF
pre-migration
24 hrs

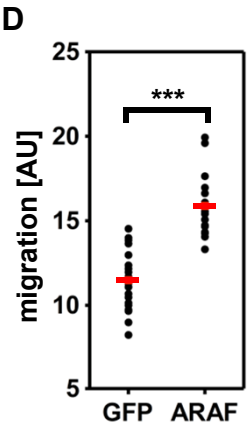
D
migration [AU]
***
GFP
ARAF

Figure 7

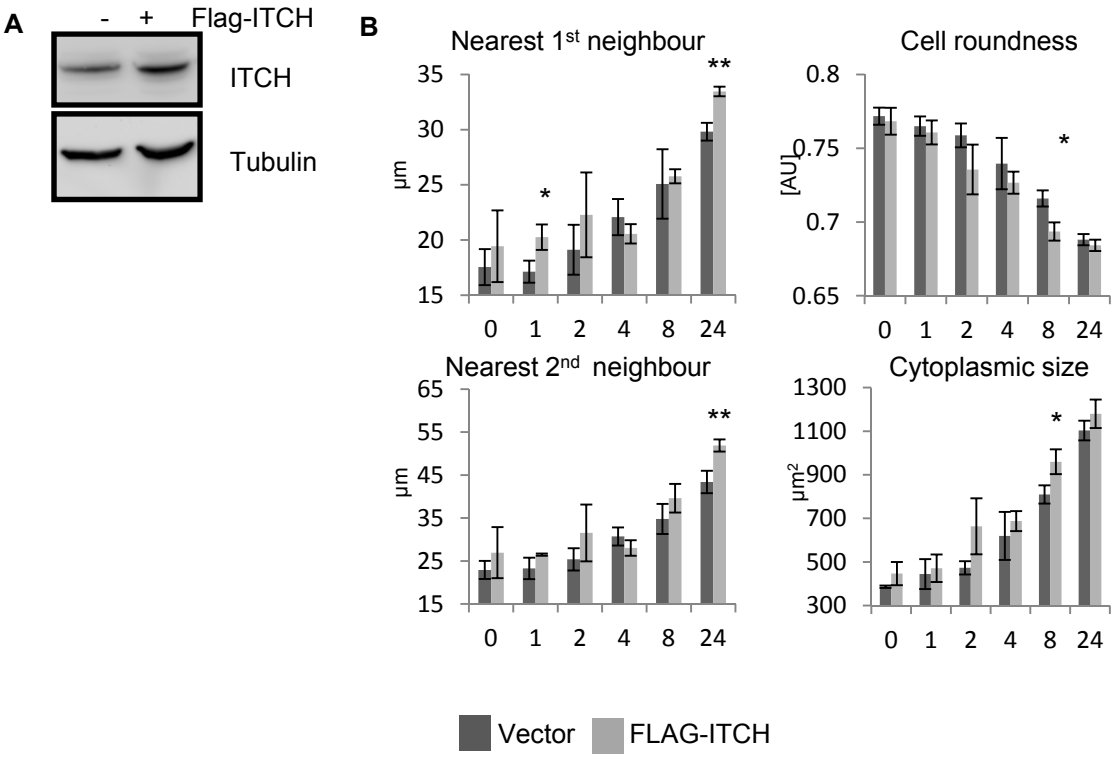
A
- + Flag-ITCH
ITCH
Tubulin
B
Nearest 1st neighbour
µm
35
30
25
20
15
0 1 2 4 8 24
*
**
Cell roundness
[AU]
0.8
0.75
0.7
0.65
0 1 2 4 8 24
*
Nearest 2nd neighbour
µm
65
55
45
35
25
15
0 1 2 4 8 24
**
Cytoplasmic size
µm2
1300
1100
900
700
500
300
0 1 2 4 8 24
*
Vector
FLAG-ITCH

Figure 8

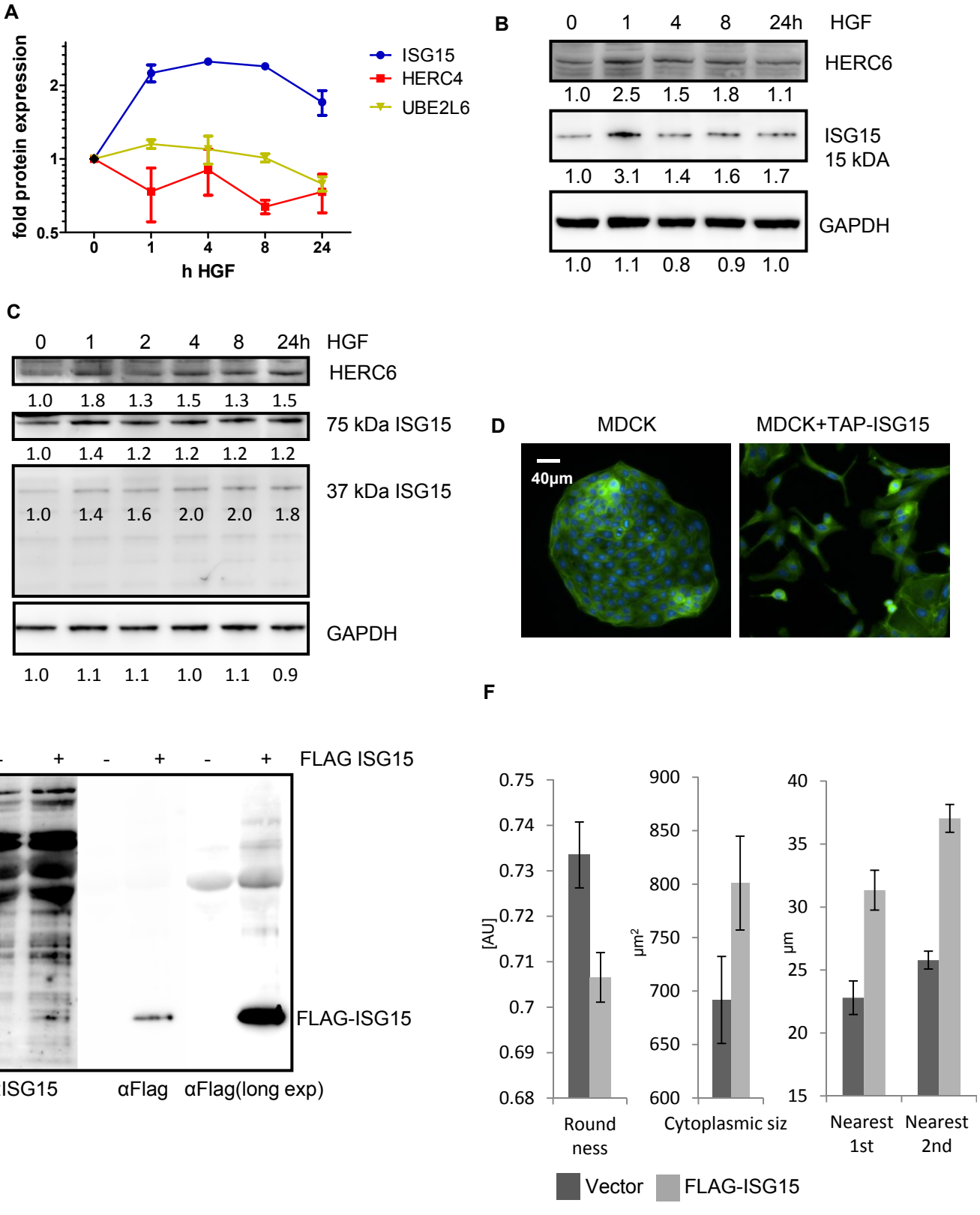
A
fold protein expression
2
1
0.5
0
1
4
8
24
h HGF
ISG15
HERC4
UBE2L6
B
0 1 4 8 24h HGF
HERC6
1.0 2.5 1.5 1.8 1.1
ISG15
15 kDA
1.0 3.1 1.4 1.6 1.7
GAPDH
1.0 1.1 0.8 0.9 1.0
C
0 1 2 4 8 24h HGF
HERC6
1.0 1.8 1.3 1.5 1.3 1.5
75 kDa ISG15
1.0 1.4 1.2 1.2 1.2 1.2
37 kDa ISG15
1.0 1.4 1.6 2.0 2.0 1.8
GAPDH
1.0 1.1 1.1 1.0 1.1 0.9
D
MDCK
MDCK+TAP-ISG15
40µm
E
- + - + - + FLAG ISG15
FLAG-ISG15
αISG15
αFlag
αFlag(long exp)
F
0.75
0.74
0.73
0.72
0.71
0.7
0.69
0.68
[AU]
Round ness
900
850
800
750
700
650
600
µm²
Cytoplasmic siz
40
35
30
25
20
15
µm
Nearest 1st
Nearest 2nd
Vector
FLAG-ISG15

Suppl Fig S1

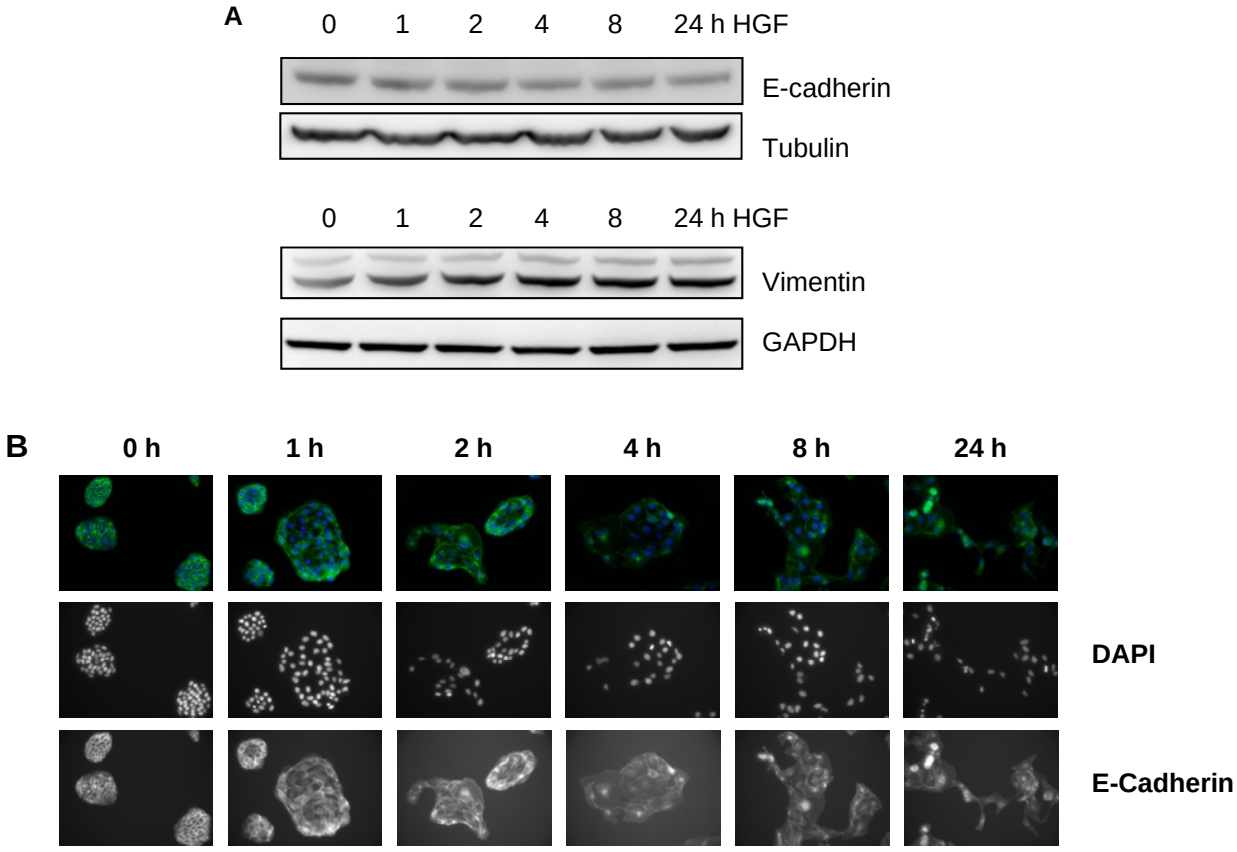

Supplementary Fig. S1. E-cadherin internalization A. MDCK cells were treated as indicated, lysed, electro-blotted, detected with antibodies as indicated and imaged on a CCD-camera. **B.** Epi-fluorescent image of E-cadherin localisation. MDCK cell were treated with HGF accordingly, fixed and stained with DAPI (blue) or an anti-E-cadherin antibody detected with an anti-rabbit Alexa488 labelled secondary antibody (green).